Answers to the comments on acp-2020-40

A Microphysics Guide to Cirrus – Part II:
Climatologies of Clouds and Humidity from Observations

by Krämer et al.

First of all, we like to thank the two referees a lot for their very positive rating of the manuscript and also for the constructive comments that further improved it. We are aware that the paper is very long and comprehensive, but could still have been extended into several directions. It was not easy to find a good balance in summarizing earlier findings and adding new data analysis, and we are glad to see that the work that went into the study seems to have led to a satisfactory result.
In the following, we answer point by point the comments of the referees (colored in black), our answers are blue.

One thing we would like to mention before the responses to the refrerees: unfortunately, an error was found in the calculation of the hours of the observations, so that the number of plotted data did not always match the calculated number of hours. This has been corrected. In the plots of clear sky RH_{ice} and H_2O, also the data numbers have changed. This is also corrected in the new version of the manuscript. The changes do not affect the scientific contnet of the Figures. However, we apologize for this mistake.

Anonymous Referee #1

This manuscript presents a comprehensive review of airborne in-situ and satellite re mote sensing climatologies of cirrus clouds and water vapour. It combines previous as well as new insitu databases that help clarify detailed properties of tropical and mid- latitude cirrus and their responses and across a very important altitude range 5-20km. The links to satellite-borne data sets offers a benchmark for the model community to identify and begin to improve uncertainties in cirrus feedbacks → We are glad to read hat, this is what we had hoped to be able to provide.

The scale of the database and attention to detail is an impressive, particularly with respect to the review and update of in situ database quality control for known and ongoing issues with respect to small ice quantification due to artefacts in measurements. This is particularly important in assessing error contributions to small ice concentrations providing confidence in the interpretation of different cirrus generation mechanisms currently being discussed, in-situ and liquid origin processes. These are well described although there is still much to be understood. The summary section on characteristics and distribution of in-situ origin and liquid origin cirrus linked to the previous Kramer et al. publication is very useful and helps to clarify the very large, sometimes overwhelming data sets. Despite some of the issues with previous measurements/data sets I found Figure 4 e.g. very encouraging showing a consistent relation between cirrus ice crystal concentration and mean ice mass radius and ice water content IWC.

The limitations of the data sets are discussed in good detail ins section A2.2 which is an important point for data users to be mindful of due to the impact on the uncertainties on concentrations/counting statistics and frequencies of occurrence of small cirrus ice crystals due to the very different sample volumes of the different instruments used in the analysis. Improving instrument response for small ice crystals still remains a challenge for in situ instruments especially for non-grey-scale imaging probes so merging data sets under varying environments needs to be treated with caution. The key issues are however explained - integration times dictated by different instrument sample volumes might limit detection of cirrus spatio-temporal inhomogeneities and hence interpretation of formation mechanisms. It was good to see the possible effects of this

discussed and also those due to ice shattering (Figure 18 e.g.) which provides a useful benchmark for new data sets to compared with.

Figures 5 and 6 presented a nice overview of the data sets and how the different formation mechanisms contribute (minor typo in the Figure 5 legend, "summery" should be summary: → corrected) versus clear sky conditions and as a function of region. Minor typo Figure 7, plate Nice vs T, Nice units given as 1/ccm. This should be changed to cm-3 to be consistent with previous and subsequent figures. Fig. 7 is copied from Krämer et al., 2009, so changes are not possible now; for information: the Figure is moved to the supplementary material in the revised version.

The final results are perhaps not surprising and consistent with previous - i.e. "across all latitudes, the thicker liquid origin cirrus predominate at lower altitudes, while at higher altitudes the thinner in-situ cirrus prevail." However, this study does provide a comprehensive database with estimates of radiative forcing ranges constrained by well described uncertainties.

Whilst this paper is extremely long and comprehensive it would have been useful to height potential uncertainties in some satellite retrievals, particularly with regard lack of sub-cloud top processes but likely this is not an issue for many of the cirrus discussed here.

All in all this is an excellent and very comprehensive review and analysis of our understanding of cirrus. Thanks again !!

Anonymous Referee #2

This article reports findings of cirrus microphysical properties (IWC, Nice, Rice) and humidity from a climatology constructed from a large amount of airborne measurements, covering latitudes from 20S to 75N. This impressive data archive has been carefully quality checked and includes 150 flights from 24 campaigns. This effort is a huge contribution to our field. It is extremely difficult to build an unbiased climatology from airborne measurements as they often exist only for specific regions and at specific seasons. Results are presented as function of altitude and temperature, also stratified by tropics and NH midlatitudes (Sections 3 and 4). The supplement presents separate results for each of the 15 campaigns added to the ones of an earlier publication. Special attention has been given to the TTL of the Asian monsoon, using recent measurements of the StratoClim campaign (Section 5). A second important part of this article consists of using these measurements to rescale ice crystal number concentration retrieved from global satellite radar-lidar observations, which then allows to compare Nice of different latitude bands (Section 6), in the case that this scaling factor of 1.73 is valid over the whole IWC-T range and over the whole globe.

This is a highly important article and should be published after revision. The abstract, introduction and conclusions are well written. It is really not an easy task to synthesize so much information. The present form of the article, though already quite well synthesized, is long, with a multitude of figures. The article could gain in clarity by taking into account the following suggestions. In particular, as already in Part I the cirrus clouds have been classified as in-situ and liquid origin and here are further distinguished according to updraft strength, a presentation of the in-cloud properties Nice, Rice and RHice in the IWC-T space, instead of only in the T space, would be very helpful.

Thank you very much for this suggestion, we have added a respective new Figure (new Figure 6) and a new Section (new Section 4.1) to the manuscript. Such a representation of the data was not included in the first version of the paper, since we had already discussed the structure of Ni and Ri in the IWC-T space in Part 1 of the paper, but not as percentiles in IWC-T intervals. We were

surprised how informative this new new analysis is and think that it might become one of the more noted result of the paper.

Major comments:

0) Sections 3 and 4 both present results of the airborne climatology, with many figures. In general 6 variables, 3 corresponding to cirrus microphysical properties (IWC, Nice, Rice) and 3 corresponding to humidity (in-cloud RHice, clear sky RHice and clear sky water vapour mixing ratio) are presented stratified by altitude, latitude and temperature in these two sections. I would merge these sections into one section (3. In-situ climatologies), with for example subsections 3.1 Latitude – altitude distributions (including description of Figure 2), 3.2 In-cloud properties stratified by T and by (IWC, T), 3.3 In-situ and liquid origin cirrus.
There are long descriptions, and as the tile includes the word 'Guide', the behaviour of Nice, Rice and RHice in the IWC-T space, instead of or in addition to in the T space alone, would probably be clearer in respect to the cirrus classification. Therefore this new section 3.3 should show IWC as function of T (as already in Figs. 6-10), but then the other in-cloud properties as function of IWC and T (median or mean in IWC/T intervals and also variability in IWC/T intervals). The presentation in the (IWC-T) space has several advantages:
1) one can probably better distinguish the different types of cirrus and their the properties Nice, Rice and RHice, leading to a more quantitative Table 1, and
2) this would be a very useful synthesis for testing parameterizations in climate models, as recent bulk ice cloud schemes rely on both of these parameters, IWC and T (see for example Field et al., 2007; Furtado et al., 2015; Baran et al. 2016 or Figs. 4f-h of Stubenrauch et al., 2019).

Response to 0:
We see and also like the idea behind the proposed structuring, namely to first consider entire climatologies of median values of the parameters (and their deviations) in the latitude-altitude and the T-IWC parameter space (and maybe also the frequency distributions of the parametrs versus temperature) and then to split the climatologies into the two cirrus types, in-situ origin and liquid origin.

What would be lost in such a version of the article would be the discussion of the microphysical processes and the identification of the types based on the representation in Figure 3 (individual data points). If one calculates medians in intervals, characteristic differences that are important for this type of interpretation disappear.

We also like to note here that the two different types of cirrus can not be distinguished looking at medians of Nice, Rice and Rhice in the T-IWC space (see new Figure 6, for convenience added at the end of this document) because of the overlap of the types in the T-IWC space. For such an analyses it would be necessary to first split the data set into in-situ-origin and liquid-origin cirrus and then produce the median T-IWC plots (as done by Luebke et al., 2016 and Wolf et al., 2018, 2019 for specific field campaigns). Such a sorting of the database is difficult (because the trajectory based method does not work in convective systems) and an ongoing work in our group. We will be happy to present such plots and also a more quantitative Table 1 (some quantification is given there, see answer to point 5)) in a future publication.

The division of the paper into sections 3 and 4 followed the idea of first discussing the microphysical processes and characteristics of the cirrus types and then moving on to climatologies of the frequencies of occurrence, which can also be used to test parameterizations in climate models or satellite retrievals.

As a synthesis of our aproach and the new and very informative ideas of the referee, we kept Sections 3 and 4, but
- added altitude-latitude plots of interval percentiles of the 6 variables (Section 3) as supplementary material (new Figures S1 – S3),

- added T-IWC plots of Nice, Rice, RHice of interval percentiles (Section 4) as supplementary material (new Figure S4); we further added T-IWC plots of DARDAR-Nice medians (Section 6) to the supplementary material (new Figure S5),

- added a new Subsection to Section 4 (4.1: The IWC-T parameter space: median Nice , Rice , Rhice), where the T-IWC plots of Nice, Rice, RHice interval medians are discussed (new Figure 6, see also at end of this document).

Merging some of the figures as follows.

1) Figure 2 should only show 3 of the 4 sub-figures which links altitude and temperature for different latitude bands (one could imagine to separate summer and winter midlatitudes). What are the different colors within one latitude band? The right panel seems to be only an example from one field campaign (perhaps one could move this to section 5 where the TTL is discussed, or as it is published one can just resume the conclusion in the text).

Response to 1:
- We have not splitted the data set into winter and summer because to our feeling the in-situ data base is still not large enough to proviede a view on seasons. This Figure should give an impression on the temperature, Theta and altitude ranges of the different geographical regions, so we decided to use the Figure published earlier.

- The colors are: blueish colors for Arctic, greenish colors for mid-latitude and reddish colors for tropical observations, which is mentioned in the Fgure caption.

- We agree with the referee and removed the right panel.

2) Figure 3 presents scatter plots of these 6 variables deduced from all measurements, as function of altitude and latitude. The information could be presented in a more quantitative way by building intervals in altitude (for example per km) and per 10◦ in latitude and plot then the averages or medians in these intervals (and in addition the variability within the intervals in a separate plot), instead of superposing each of the measurement which indeed shows the scatter but also leads to confusion as some of the points are below others. It looks to me that the most rare measurement values are plotted above so that one can see them (in blue). The comments on the figures are very interesting, but the color blue should only be used if they correspond to the color of the variable value.

Response to 2: To better explain the way we have plotted the data we have added new text at the beginning of Section 3.1:

‚The way the data is presented here as individual points was chosen because the entire range of measurements is visible. Although data overlap occurs in this type of display, it is possible to identify cirrus types and microphysical processes, especially based on extreme values. As additional overview information, we have created latitude-altitude intervals (0.5◦ latitude, 500 m altitude) and calculated the 25, 50 (median) and 75 % percentiles for all variables. These additional altitude-latitude climatologies are shown in the supplementary material.‘

and also in Section 3.1.1:
‚*Microphysical characteristics:* In the new in-situ data set, containing advanced measurements and extended by several field campaigns in comparison to the earlier studies, some typical characteristics of the cirrus types and hints to ice nucleation mechanisms are visible. In the following, the cirrus types are briefly introduced, and, using Figures 3 and 4, the types and freezing mechanisms are discussed and summarized in Table 1.‘

3) Then in Section 4, these 6 variables are shown as function of T in Figures 6 to 9.

Take out Figure 7 (earlier results, already in supplement as Figure 1), (done)

and build two figures, 6 and 7:
- new Figure 6 could present IWC as fct of T, and Nice, Rice and RHice in IWC-T space, for all (done, **see Response to 0** and new Figure 6, also at the end of this document),
- NH midlatitudes and tropics (we have produced these plots, but they look very similar to the plot for all data -except of the temperature range- **** ,** so we decided not to show them to not further lengthen the paper), and
- new Figure 7 H2O clear sky as fct of T and perhaps RHice clear sky in H2O-T space, for all, NH midlatitudes and tropics. (also for the sake of brevity, we have not shown such plots since they do not provide additional information)

One motivation of this analysis is certainly to verify that there is a coherent relationship between the microphysical values and T (this is discussed now in new Subsection 4.1), even if the tropics and midlatitudes include cirrus with a different range of these values. Therefore a joint discussion of all, NH midlatitudes and tropics will be easier to follow (see comment ****** above).

4) Section 3.1.1: As already in Part I, the authors classify cirrus according to their origin: in-situ or liquid origin; and they nicely summarize their characteristics by further distinguishing those meteorological situations with slow and fast updrafts. However, it is not clear to me from where the authors have the information on the updraft speed. Is this based on simultaneous measurements or on intuition? As this classification is one of the core findings, it is important to explain from where this information is obtained.

Response to 4:
Good point, thanks for noticing this - sometimes one is routine-blinded as a author … we note now that the division in slow and fast updrafts is at ~10cm/s, based on simulations presented by Kärcher and Lohmann (2002) and Krämer et al. (2016).

5) I would place Table 1 at the end of Section 3, so that the words ‘low’, ‘few’, ‘large’, etc. can be replaced by ranges (probably separately for tropics and midlatitudes). The authors show ranges in Figure 5, but these are only for midlatitudes, (probably at equinox conditions, as they were used for a specific simulation).

Response to 5:
Since we have kept the structure of the Sections, we have not moved Table 1. Please note that ranges of 'low', 'few', 'large', etc. are given in the text below the Table:

slow updraft: $\lesssim$ 10 cm/s; *fast updraft:* $\gtrsim$ 10 cm/s (Kärcher and Lohmann, 2002; Krämer et al., 2016).
IWC high/low: above/below the IWC median (see Figure 7).
N_{ice} few/more/many: below/in-between/above the 10 and 90% N_{ce} percentiles (see Figure 7).
R_{ice} small/large/larger:
ice particles $\lesssim$ 20µm dominate the PSD /
ice particles $\gtrsim$ 20µm dominate the PSD, max. size several hundred µm diameter /
ice particles $\gtrsim$ 20µm dominate the PSD, max. size up to thousand µm diameter,
PSD: particle size distribution.

6) Section 6: Section 6.1 presents an evaluation of the remote sensing lidar-radar retrieval method, by comparing Nice in the T space from in-situ PSD measurements of 5 campaigns and Nice in the T space, where in a first step N0* and Dm, assuming a modified Gamma function, have been determined from these in-situ PSD data to use them as a constraint in the satellite retrieval (Figure 13). An interesting finding of the comparison between the two Nice results is that the Nice overestimation from satellite retrieval can be partly explained by the fact that the in-situ PSDs often do not contain ice crystals with D < 20 micron, while the retrieval assumes a PSD including all size bins (lines 750-751). This bias should be larger at low T. However, in Section 2.2 it is written that for T > -50◦C (220 K), an overestimation in DARDAR-Nice is due to the inability of the modified Gamma distribution to match the frequently bi-modal shape of measured PSDs (lines 149-151). This statement means that at warmer T there is also an overestimation, but for a different reason. Should this not be discussed when considering Figure 13? And should then not follow, that a different scaling factor applies for T < 220 K and for T > 220 K? Unfortunately the logarithmic scale and the squeezed y axis do not permit to see if two instead of one scaling factor over the whole T range would be better.

Response to 6 start:
This is a very good point raised by the reviewer, which refers to an attempt to correct inherent biases in statistical comparisons of Ni from satellite (DARDAR-Nice) and in situ observations. Learning from preliminary comparisons by Sourdeval et al (2018) between the satellite (DARDAR-Nice) and a subset of the current in-situ dataset (5 campaigns) led the authors to identify two main effects that can lead to possible biases.

The first is due to the assumption of a mono-modal PSD in the satellite algorithm, which becomes limiting when ice particle growth processes are dominant, and leads to an overestimation of Ni in DARDAR-Nice. However, the -50°C threshold announced by Sourdeval et al (2018) is very conservative. While bi-modality indeed appears from this temperature, the impact on Ni is not substantial. Their study even showed a reasonably good agreement of the satellite Ni and co-located in situ observations down to T = -30°C (see Fig. 4 of that paper). It is therefore reasonable to consider that DARDAR-Nice is capable of retrieving Ni with only small biases due to bi-modality of the PSD for the entire range of cirrus temperatures observed here, while keeping in mind that an overestimation of Ni is possible for certain cloud types.

The second effect that of the continuity of PSD bins, that is assumed by the satellite algorithm from 5 um and is not necessarily guaranteed in the in-situ data. This concerns mainly small ice crystals, which significantly contribute to Ni, and leads to a higher Ni in the satellite retrievals. The understanding of the physical basis for these missing or empty bins is a very interesting question, which will require further investigation. For the moment, this manuscript proposes to correct this issue by using a scaling factor applied on the satellite Ni.

It can be noted that both effects are not expected to affect the same temperature ranges, as cold temperature would lead to a higher satellite Ni due to missing/empty PSD bins and warmer would lead to higher satellite Ni due to PSD bi-modality. This leads us to agree with the reviewer that a temperature dependent correction would be optimal. However, considering the large uncertainties on our understanding of these effects, and probably the occurrence of other issues that might lead to other biases (e.g. the PSD shape assumed in the retrievals), we decided to use the simplest option of a single scaling factor over the entire temperature. This choice appears very reasonable from Fig. 13, especially considering the large Ni variations around the overall median. This choice still appears to us as being the most reasonable and adapted for this paper, until more can be understood on these effects.

The text in section 2.2 has been clarified to account for this comment:
„Good agreements were found, except for temperatures higher than about -50°C where an overestimation in DARDAR-Nice due to the inability of the modified gamma distribution to match the frequently bi-modal shape of the measured PSDs."
replaced by
„Good agreements were found, although it was noted that the inability of the modified gamma distribution to match the frequently bi-modal shape of the measured PSDs could lead to an overestimation of Ni in DARDAR-Nice. This typically occurs at temperature above -50°C and is expected to be cloud-type dependent, but Sourdeval et al (2018) showed that Ni still was in reasonable agreement with the in-situ (a factor of 2) down to T = -30°C, which should cover the entire cirrus temperature ranges in this study."

6) ctd. 1: Again, I suggest to present Nice also in the IWC-T space, especially since IWC is also available from the DARDAR retrieval. Same for Figures 14 and 15. Then it could be directly seen that the thinnest Ci at cold T are not detected by DARDAR, and perhaps even that different scaling factors would apply in different (IWC-T) intervals.

Response to 6 ctd. 1:
The display of Ni in a IWC-T space is a very good suggestion, as it clearly allows for a better visibility. This approach is now used in Fig. 6 of the revised manuscript and an equivalent for DARDAR-Nice is here shown. Due to limited space, this figure has been included in the supplements of the revised manuscript (Fig. S5). The overall agreement between DARDAR-Nice and the Cirrus Guide II data set of the distribution of Ni bins in the IWC-T leads us to believe that the first order approach of a single scaling factor in the IWC-T interval should be reasonable for the means of the study.

This following paragraph is added to Section 6:
„Note that an analysis of Ni in a IWC-T space, similarly to Figure 6, is shown in Fig. 5 of the supplementary material. This figure shows a good climatological agreement between the satellite product and the Cirrus Guide II data set, with very similar distribution of Ni in the IWC-T space. Differences could be attributed to lack of statistics in Figure~6 (noisy patterns). However, one notable difference is the slope of the IWC-T relation, which appears

much flatter in the satellite product than in the in-situ data, as indicated by the density isolines."

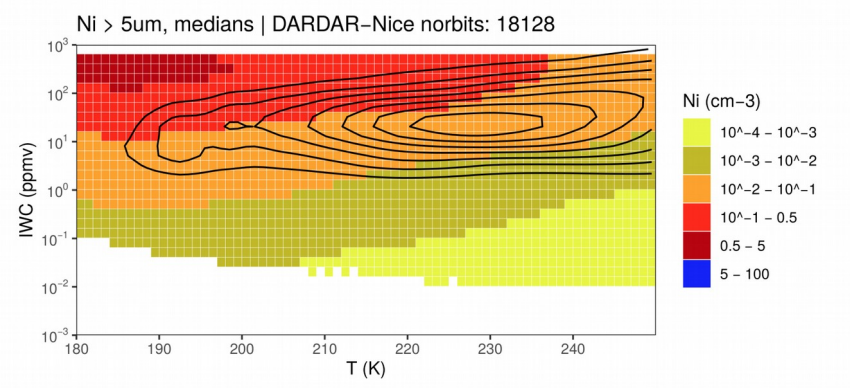

New Figure S5: Similarly to Figure 6 of the revised manuscript; Median Nice in intervals in the IWC-T parameter space for DARDAR-Nice. Densities of occurrence are indicated by plain isolines.

6) ctd. 2: For the analysis in Figure 13, N0* and Dm ware determined from the in-situ data and used as constraint for the satellite retrieval, rather than being constrained from radar-lidar measurements during usual retrievals (line 751). I do not completely understand this sentence: does this mean that for the comparison and the following scaling, results of a special radar-lidar retrieval were used or is the global climatology, presented in sections 6.2 and 6.3, also based on the lidar-radar retrieval with this (N0*, Dm) constraint ? If the usual retrieval is different, then one should also show Nice for the usual retrieval. Perhaps this only needs clarification in the text.

Response to 6 ctd. 2: We thank the reviewer for notice this lack of clarification in the text, and we agree that further explanations are required. There is no incompatibility between the analysis in section 6.1 and those using actual retrievals in section 6.2. Unfortunately there is almost no co-incident flights between CALIPSO/CloudSat and the in-situ flights, and so an indirect method had to be used to identify biases due to incompatibilities between DARDAR-ice and the in situ data. In section 6.1 we assume that the N0* and Dm retrievals are ``perfect'' in the sense that the lidar-radar measurements would have had sufficient information to perfectly retrieve the in-situ-measured N0* and Dm parameters. There is no further difference to the usual retrieval method. This approach allows to by-pass the measurement sensitivity issues and directly identify incompatibility issues in the satellite algorithm, i.e. here the limits of using a monomodal shape and the lack of missing/empty bins below 25 um. Sourdeval et al (2018) completed this theoretical analysis with actual co-

incident flights from SPARTICUS (not included in the in-situ data) and showed that its conclusions still hold when looking at actual retrievals.

Line 751 was completed by the following sentence: „This approach allows to identify inherent incompatibilities between the satellite retrieval assumptions and the in-situ measurements, by assuming that the in-situ PSD parameters are perfectly constrained by the lidar-radar. Therefore, possible differences should only be attributed to other retrieval assumptions, such as the PSD shape. Sourdeval et al. (2018) showed that this approach is efficient for identifying algorithmic limitations while still being representative of actual satellite retrievals."

7) Section 6: Once Nice adjusted by a constant factor 1.73, Nice is decreasing with increasing T in Figure 14, while Nice is constant with T for in-situ measurements. Again, the presentation of Nice as fct of IWC and T and its variability within the IWC-T intervals will perhaps give additional insight, in particularly if one distinguishes tropics, midlatitudes and polar regions.

Response to 7:
Nice from the satellite dataset actually decreases with increasing T even without the adjustment factor 1.73, but this indeed shows a possible issue in the way the satellite data is scaled. As the reviewer indicates, this factor most likely depends on the temperature at least, but also on the IWC and more generally on the ice cloud regime and nucleation type. The „correction" applied in this manuscript clearly is a first-order attempt to make satellite and in-situ data more compatible under direct comparisons for the means of this study, and is already giving good results in section 6. We completely agree that this correction is limited and should further expanded, but this would require many more analyses that would make the manuscript too dense. We nevertheless keep in mind this important comment by the reviewer for a future study, as understanding of these difference and the „bias" between satellite and in situ data is an important step towards improving our general understanding of ice cloud remote sensing or even processes (e.g. are the missing/empty bins a satellite or in-situ issue?).

The following sentences are added at the end of section 6.1: „A correction that depends on temperature, and possibly IWC, might therefore be optimal but a simpler first-order correction of 1.73 for all T and IWC range should here be sufficient for the needs of this study and considering the multitude of processes that can lead to this bias. Future studies will be required to precisely understand such inherent differences between satellite and in-situ dataset."

On the other hand, the discrepancy between the DARDAR-Nice and in-situ Nice median can be caused by the underlying flight strategies of the in-situ measurements. In Section 6.2, we wrote:
‚We attribute the slightly increasing median Nice with decreasing temperature to homogeneous ice nucleation events, because homogeneous ice nucleation rates increase with decreasing temperature, but their appearance in space and time is transient, as discussed in Section 4.2.2. Thus, such events are difficult to find by research aircraft. Hence, these events are likely underrepresented in the aircraft observations.‘

8) Section 7: lines 952-953 (conclusions from Figure 5): The authors should make it very clear that the analysis in Figure 5 only serves as an illustration how this data archive can be used

to determine cloud radiative effects. The presented radiative transfer calculations have only been undertaken for a specific situation: at noon, equinox, at 50◦ latitude, only representative for midlatitude conditions at a specific daytime. This should be clearly written in the conclusions. It is mentioned as a kind of footnote in the legend of Figure 5, but can be easily overseen.

Response to 8 start:
In the conclusions, we changed the sentence
‚Finally, a first estimate of the radiative characteristics of typical idealized in-situ and liquid origin cirrus scenarios is given (Figure 5)' to
‚Finally, a first estimate of the radiative characteristics of typical, specific idealized in-situ and liquid origin cirrus scenarios is given (Figure 5)'.
This is also discussed in the main text in Section 3.1.1., new page 12, lines 352-355.

Also, there have been many studies on cirrus radiative effects published before, it might be interesting to compare with earlier results (for example Kienast-Sjögren et al., 2016 or Campbell et al., 2016).

Response to 8 ctd.:
We added a comparison with Kienast-Sjögren et al., 2016 and Campbell et al., 2016, the new paragraph (page 12) reads now:
„ ..., the slow 'in-situ origin' cirrus have only small optical depth (τ) between 0.001 - 0.05, resulting in a slight net warming effect of not larger than about 1.5 W/m2. The optical depth of fast 'in-situ origin' cirrus is larger (τ : 0.05 - 1), but most of them are also warming (2-10 W/m2). The thickest fast-updraft 'in-situ origin' cirrus at the lowest altitudes change the sign of their net forcing, they switch to a slight cooling effect. The reason is the warmer temperature at lower altitude that reduces the warming effect of the longwave infrared radiation. The results of the radiative forcing calculations for the slow and fast updraft cirrus are in agreement with investigations from lidar observations reported by Kienast-Sjögren et al. (2016) and Campbell et al. (2016), who observed cirrus with optical depth up to 1 and 3, respectively, and found a decreasing warming effect with decreasing optical depth. Campbell et al. (2016) even reported a slight cooling effect at the warmest observed cirrus. The 'liquid origin' cirrus, however, mostly found in the warmest cirrus layers, have large optical depths (τ : 1 - 12), which is larger than the range of cirrus optical depth reported in many studies (the maximum optical depth is often found to be 1-3, e.g. Sassen et al., 2008; Kienast-Sjögren et al., 2016; Campbell et al., 2016; Mitchell et al., 2018, ; note that this is likely because the lidar technique, often use to investiagate cirrus cloud optical properties, has restrictions in the detection of thicker ice clouds). A consequence of the large optical thickness is a quite strong net cooling effect (- 15 to -250 W/m2) of 'liquid origin' cirrus. These values are of the same order of magnitude as reported from direct measurements inside of cirrus clouds (Wendisch et al., 2007; Joos, 2019)."

9) Will this data archive be made available? I did not find a section about data availability.

Response to 9:
Yes, after acceptance of the paper, in the final version of the manuscript, a link will be included where the data can be downloaded.

Minor comments:

- Abstract, lines 22/ 23: half of the cirrus are located in the lowest warmest cirrus layer; what is the warmest cirrus layer?

We added the temperature range (224-242 K).

- Section 2, lines 120 – 124: the data of 4 campaigns out of 24 campaigns are not used, because the data volume is too low or too high. If the data volume is too high, one could imagine to filter out cases randomly. It is a pity that the data are not used at all. Or did I understand something wrong? Are all following results based on the 20 campaigns?

Yes, the following results are based on the 20 field campaigns. The reason not to include the two larger data sets was that during theses campaigns mainly similar meteorological situations with very thick liquid origin cirrus were sampled, which would have biased the statistical analysis. To include only some filghts would have been an option to include some of the data – we are sorry that we have not thought about that. On the other hand, we believe that this would not have changed the overall picture that we presented.

- Section 2.2: It was found that the assumption of a modified Gamma distribution for the PSD is only valid for T < -50◦C, which limits the statistics very much, and which leads to a positive bias of Nice at warmer T, because the assumed PSD shape is not coherent with observed bimodal PSDs. Are there other assumptions in the retrieval which may lead to biases?

There are indeed other PSD assumptions that might lead to biases between the satellite and in-situ dataset. Notably, the choice two fixed parameters was until now not discussed. We have included the following paragraph in Section 6.1:

„Other assumptions on the PSD shape by the satellite remote sensing method might also contribute to this bias. The PSD shape indeed is provided by 4 parameters, 2 of which are fixed and 2 are retrieved (see Section 2.2). Delanoe et al. (2014) showed that the two fixed PSD parameters defined by Delanoe et al. (2005) and used in DARDAR-Nice might lead to a too steep representation of the small ice mode (i.e. too high Nice) and should be updated in future algorithm versions. Also, the bi-modality of the PSD towards temperature where growth processes become important is not accounted for and usually leads to small positive Nice biases (Sourdeval et al. 2018). The cause of these assumptions are difficult to account for, as they most likely depend on the cloud-type and on the thermodynamical environment, but they should on a first order be reasonably captured by the 1.73 adjustment factor."

- Figure 13: It is not clear which satellite retrieval statistics is used: only the regions and seasons of the 5 campaigns? This needs some explanation in the text.

As indicated in the figure caption and in the second paragraph of section 6.1, only the five mentioned campaigns are used in Figure 13. As shown in Figure 1, these campaigns are representative of a tropical and mid-latitude ice cloud. The following sentence was included in Section 6.1 for better clarity:

„This section therefore focuses on these five campaigns, which are nevertheless representative of a wide range of mid-latitude and tropical ice clouds (see Figure 1 and caption of Figure 13)."

- Figure 1: are the airplane schemes necessary? It is nearly impossible to read the name of the campaigns. As there are no flights in the SH higher latitudes, one could use this space to write these names there, which allows to increase the size of the map.

The airplane pictures are not essential, however, we think it gives an of impression on the experimental work to operate cloud and water vapor instruments on so many different platforms. We have enlarged the Figure to the maximum size and hope that zooming in might help to read the campaign names.

- Section 5: Figure 10 is already in the supplement. As this section concentrates on the Asian monsoon, the data of Figure 10 can be analysed in the IWC-T space as proposed above.

In Section 5, the special features of occurence frequencies appearing in Figure 10 (Asian Monsoon) in comparison to the entire tropical climatology are discussed. We repeated this Figure in the Supplementary Material for the sake of completeness, so that one do not need to flip back and forth between main paper and supplement when looking at single campaigns. Thus, think that it is useful to keep the Figure as is.

- Title of Section 6: Global cirrus Nice climatology from satellite remote sensing (the regional data are included in the global)

Changed.

- Table 3: could one add Nice for tropics and NH midlatitudes from in-situ measurements?

The median Nice in this Table are calculated for the entire spatial and temporal Nice-T parameter space shown in Figure 15. This is possible for remote sensing measuremenst which are able to scan the entire space. In-situ observations provide only a snapshot of the statistical Nice distribution, thus medians from the entire Nice-T are not representative (see also text on page 29, lines 978 ff).

- Typo, line 188: distribution of cirrus

Changed.

- Typo, line 409: which can be seen

Changed.

- Typo in Table 2: median for 190K-200K: 0.100 instead of 0.010

Changed.

References mentioned in 1. Paragraph of major comments:

Field, P. R., Heymsfield, A. J., & Bansemer, A. (2007). Snow size distribution parameterization for midlatitude and tropical ice clouds. J. Atmos. Sci., 64, 4346–4365, doi:10.1175/2007JAS2344.1.

Furtado, K., Field, P. R., Cotton, R., & Baran, A. J. (2015). The sensitivity of simulated high clouds to ice crystal fall speed, shape and size distribution. Q. J. R. Meteorol. Soc., 141, 1546-1559, doi:10.1002/qj.2457.

Baran, A. J., Hill, P., Walters, D., Hardiman, S.C., Furtado, K., Field, P.R., & Manners, J. (2016). The Impact of Two Coupled Cirrus Microphysics–Radiation Parameterizations on the Temperature and Specific Humidity Biases in the Tropical Tropopause Layer in a Climate Model. J. Climate, 29, 5299–5316, doi: 10.1175/JCLI-D-15-0821.1. Stubenrauch, C. J., Bonazzola, M., Protopapadaki, S. E., & Musat, I. (2019). New cloud system metrics to assess bulk ice cloud schemes in a GCM. J. Advanc. Model. Earth Systems, 11, 3212–3234. https://doi.org/10.1029/2019MS001642.

References mentioned in last paragraph of major comments:

Campbell, J.R., S. Lolli, J.R. Lewis, Y. Gu, and E.J. Welton, 2016: Daytime Cirrus Cloud Top-of-the-Atmosphere Radiative Forcing Properties at a Midlatitude Site and Their Global Consequences. J. Appl. Meteor. Climatol., 55, 1667–1679, https://doi.org/10.1175/JAMC-D-15-0217.1

Kienast-Sjögren, E., Rolf, C., Seifert, P., Krieger, U. K., Luo, B. P., Krämer, M., and Peter, T.: Climatological and radiative properties of midlatitude cirrus clouds derived by automatic evaluation of lidar measurements, Atmos. Chem. Phys., 16, 7605–7621.

New Figure 6:

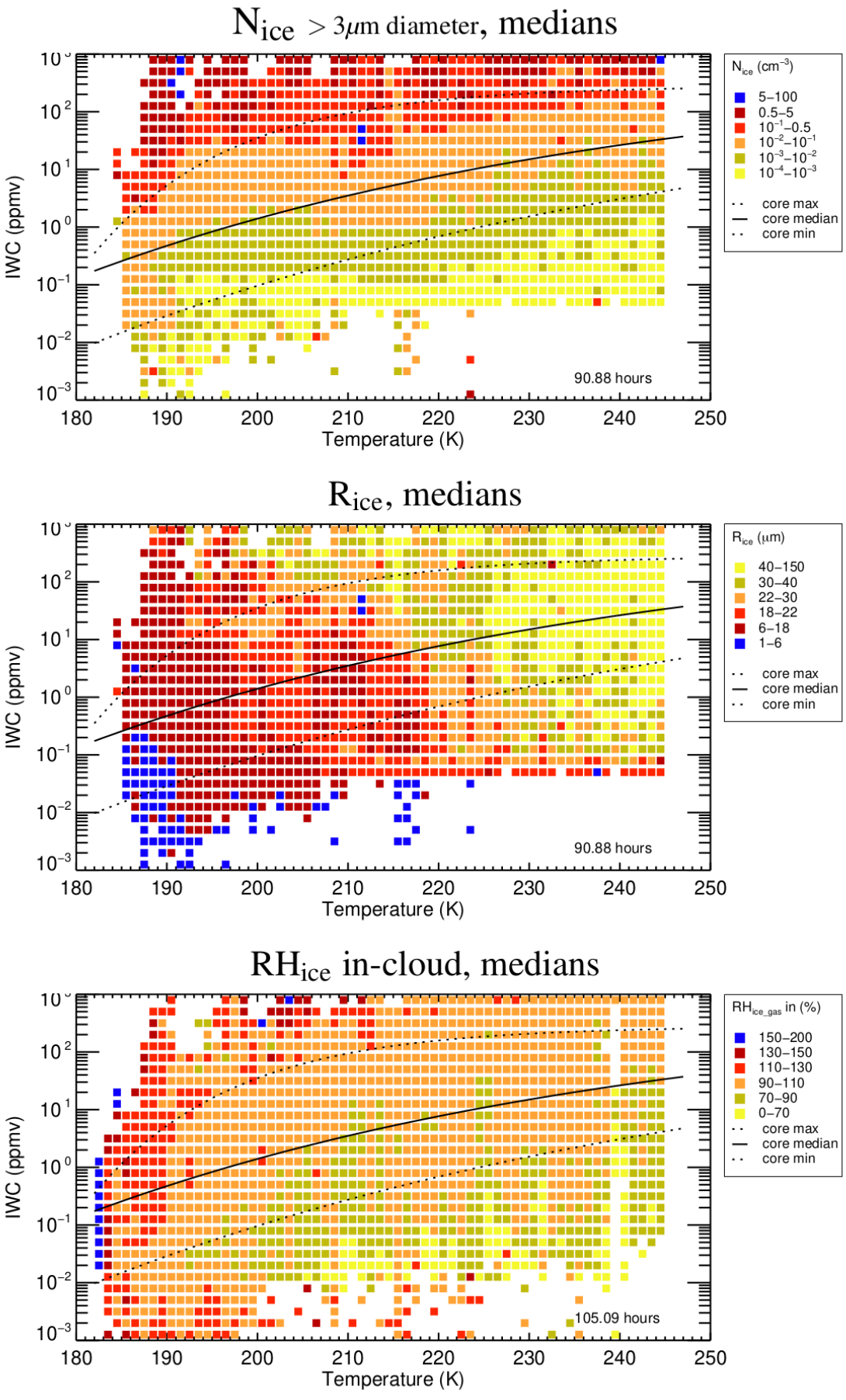
N_{ice} > 3μm diameter, medians
IWC (ppmv)
Temperature (K)
N_{ice} (cm^{-3})
5–100
0.5–5
10^{-1}–0.5
10^{-2}–10^{-1}
10^{-3}–10^{-2}
10^{-4}–10^{-3}
core max
core median
core min
90.88 hours
R_{ice}, medians
R_{ice} (μm)
40–150
30–40
22–30
18–22
6–18
1–6
core max
core median
core min
90.88 hours
RH_{ice} in-cloud, medians
RH_{ice_gas} in (%)
150–200
130–150
110–130
90–110
70–90
0–70
core max
core median
core min
105.09 hours

Manuscript prepared for Atmos. Chem. Phys.
with version 2014/09/16 7.15 Copernicus papers of the LaTeX class copernicus.cls.
Date: 29 June 2020

A Microphysics Guide to Cirrus – Part II: Climatologies of Clouds and Humidity from Observations

Martina Krämer[1,2], Christian Rolf[1], Nicole Spelten[1], Armin Afchine[1], David Fahey[3], Eric Jensen[5], Sergey Khaykin[6], Thomas Kuhn[7], Paul Lawson[8], Alexey Lykov[9], Laura L. Pan[5], Martin Riese[1], Andrew Rollins[3], Fred Stroh[1], Troy Thornberry[3,4], Veronika Wolf[7,‡], Sarah Woods[8], Peter Spichtinger[2], Johannes Quaas[10], and Odran Sourdeval[11]

[1]Institute for Energy and Climate Research (IEK-7), Research Center Jülich, Jülich, Germany
[2]Institute for Atmospheric Physics (IPA), Johannes Gutenberg University, Mainz, Germany
[3]NOAA ESRL CSD, Boulder, USA;
[4]CIRES, University of Colorado Boulder, USA;
[5]NCAR, Atmospheric Chemistry Observations and Modeling Laboratory, Boulder, USA;
[6]LATMOS/IPSL, UVSQ, Sorbonne Université, CNRS, Guyancourt, France
[7]Luleå University of Technology, Division of Space Technology, Kiruna, Sweden
[8]SPEC Inc., Boulder, CO, USA;
[9]Central Aerological Observatory (CAO), Department of Upper Atmospheric Layers Physics, Moscow, Russia
[10]Leipzig Institute for Meteorology (LIM), Universität Leipzig, Leipzig, Germany
[11]Univ. Lille, CNRS, UMR 8518 - LOA - Laboratoire d'Optique Atmosphérique, F-59000 Lille, France
‡now at Brandenburg Univ. of Technology (BTU), Atmospheric Processes, Cottbus, Germany

Correspondence to: M. Krämer (m.kraemer@fz-juelich.de)

Abstract. This study presents airborne ~~in-situ and satellite remote sensing~~ in situ and satellite remote-sensing climatologies of cirrus clouds and humidity. The climatologies serve as a guide to the properties of cirrus clouds, with the new ~~in-situ data base~~ in situ database providing detailed insights into boreal mid-latitudes and the tropics, while the satellite-borne data set offers a global overview.

To this end, an extensive, quality checked data archive, the Cirrus Guide II ~~in-situ data base~~in situ database, is created from airborne ~~in-situ~~ in situ measurements during 150 flights in 24 campaigns. The archive contains meteorological parameters, ~~IWC, , , and for each of the flights (IWC:~~ ice water content ~~,~~ (IWC), ice crystal number concentration (N_{ice}~~: number concentration of ice crystals, :~~), ice crystal mean mass radius ~~, :~~ (R_{ice}), relative humidity with respect to ice ~~, :~~ (RH_{ice}) and water vapor mixing ratio ~~)~~(H_2O) for each of the flights. Depending on the ~~specific~~ parameter, the ~~data base~~ database has extended by about a factor of 5-10 compared to earlier studies. ~~One~~

As one result of our investigations, we show that the medians of N_{ice}, R_{ice} and RH_{ice} have distinct patterns in the IWC-T parameter space. Lookup tables of these variables as functions of IWC and T can be used to improve global model cirrus representation and remote sensing retrieval methods. Another outcome of our investigations is, that across all latitudes, the thicker ~~liquid origin~~ liquid-origin cirrus predominate at lower altitudes, while at higher altitudes the thinner ~~in-situ~~ in situ-origin cirrus prevail. Further, exemplary investigations of the radiative characteristics of ~~in-situ and liquid origin~~ in situ-origin and liquid-origin cirrus show that the ~~in-situ origin~~ in situ-origin cirrus only slightly warm the atmosphere, while ~~liquid origin~~ liquid-origin cirrus have a strong cooling effect.

An important step in completing the Cirrus Guide II is the provision of the global cirrus N_{ice} climatology, derived by means of the retrieval algorithm DARDAR-Nice from ten years of cirrus remote sensing observations from satellite. The ~~in-situ data base~~ in situ measurement database has been used to evaluate and adjust the satellite observations. We found that the global median N_{ice} from satellite observations is almost two times higher than the ~~in-situ~~ in situ median and increases slightly with decreasing temperature. N_{ice} medians of the most ~~frequentl~~ frequently occuring cirrus sorted by geographical regions are highest in the tropics, followed by austral/boreal mid-latitudes, Antarctica and the Arctic. Since the satellite climatologies enclose the entire spatial and temporal N_{ice} occurrence, we could deduce that half of the cirrus are located in the lowest, warmest (224-242 K) cirrus layer and contain a significant amount of ~~liquid origin~~ liquid-origin cirrus.

A specific highlight of the study is the ~~in-situ observations of tropical tropopause layer (TTL)~~ in situ observations of cirrus and humidity in the Asian monsoon anticyclone and the comparison to the surrounding tropics. In the convectively very active Asian monsoon, peak values of N_{ice} and IWC of 30 ppmv and 1000 ppmv are detected around the cold point tropopause (CPT). Above the CPT, ice particles that are convectively injected can locally add a significant amount of water available for exchange with the stratosphere. We found IWCs of up to 8 ppmv in the Asian monsoon in

comparison to only 2 ppmv in the surrounding tropics. Also, the highest RH_{ice} (120-150%) inside of the clouds ~~as well as~~ and in clear sky ~~(120-150%)~~ are observed around and above the CPT. We attribute this to the high ~~amount of~~ H_2O ~~(3-5~~mixing ratios (3 - 5 ppmv) ~~in comparison~~ observed in the Asian monsoon compared to 1.5 ~~-3~~to 3 ppmv ~~in other tropical regions. The~~ typically found in the tropics. The observed supersaturations above the CPT suggest that the water ~~exchange with~~ transport into the stratosphere is 10-20% higher than expected in regions of weak convective activity and up to about 50% in the Asian monsoon.

Contents

1 Introduction

In Part 1 of the study (Krämer et al., 2016), a detailed guide to cirrus cloud formation and evolution is provided, compiled from extensive model simulations covering the broad range of atmospheric conditions and portrayed in the same way as field measurements in the Ice Water Content-Temperature (IWC-T) parameter space. The study was motivated by the continuing lack of understanding of the microphysical and radiative properties of cirrus clouds, which remains one of the greatest uncertainties in predicting the Earth's climate (IPCC, 2013). An important result is the classification of two types of cirrus clouds that differ ~~by~~ in formation mechanisms and microphysical properties: ~~rather thin in-situ origin~~ relatively thin cirrus that form on-site below -38°C ~~, and predominantly thick~~ (in situ-origin), and thicker cirrus originating from ~~liquid clouds~~ freezing in liquid clouds (liquid-origin cirrus) that are uplifted from warmer layers farther below.

Since then, a number of studies ~~has~~ have been published that shed further light on the exploration of the high ice clouds. For example, some new studies, mostly based on aircraft or lidar observations, provide overviews and climatologies of cirrus cloud properties (Kienast-Sjögren et al., 2016; Petzold et al., 2017; Heymsfield et al., 2017a, b; Woods et al., 2018; Lawson et al., 2019) while others present a more specific view (Urbanek et al., 2017, 2018). Overviews of ~~cirrus' properties~~ the properties of

cirrus derived from global satellite remote sensing observations were also recently enhanced to include ice crystal number concentrations (Sourdeval et al., 2018; Gryspeerdt et al., 2018; Mitchell et al., 2018). Several studies make use of the concept of ~~in-situ and liquid origin~~ in situ-origin and liquid-origin cirrus, e.g. Wernli et al. (2016), investigating the occurrence of ~~in-situ and liquid origin~~ in situ-origin and liquid-origin cirrus over the North Atlantic by analyzing ERA-interim data, Gasparini and Lohmann (2016) simulating, amongst other things, the global distribution of ~~liquid origin cirrus (they name them 'detrained ice')~~liquid-origin cirrus and Gasparini et al. (2018) presenting climatologies of in situ-origin and liquid-origin cirrus as seen by the CALIPSO satellite and the ECHAM-HAM global climate model. Wolf et al. (2018) studied the microphysical properties of Arctic ~~in-situ and liquid origin~~ in situ-origin and liquid-origin cirrus from balloon-borne observations, and Wolf et al. (2019) provide a cirrus parametrization demonstrating the dependence on the origin of the clouds.

The wealth of earlier (see e.g. references in Krämer et al., 2016) and new studies ~~provide more and more~~ has provided insights into formation processes, life cycles and appearance of cirrus. Nevertheless, there are still gaps that need to be filled, on the one hand in the ~~ice process understanding~~ understanding of ice processes, and on the other ~~hand to improve~~ in the representation of cirrus clouds in climate prediction. A way to accomplish this task requires large and high quality observational ~~data bases~~ databases that can serve, for example, to evaluate global models or other data sets and ~~to derive parametrizations of cirrus clouds reliably representing the~~ be used to derive parameterizations for improved representation of different types of cirrus clouds in models (see e.g. Wolf et al., 2019). In addition, such ~~data bases~~ databases allow detailed studies of special types of cirrus that are still poorly understood, e.g. cirrus in fast updrafts as orographic cirrus or cirrus ~~in~~ at the top of strong convection.

In this study, we approach these requirements as follows: we first compile a data archive of airborne ~~in-situ~~ in situ observations which is extended with respect to earlier versions (Schiller et al., 2008; Krämer et al., 2009; Luebke et al., 2013; Krämer et al., 2016) in terms of the size of the data set that contains all parameters needed for the desired studies, i.e. meteorological parameters, ice water content (IWC), number concentration of ice crystals (N_{ice}), ice crystal mean mass radius (R_{ice}[1]), relative humidity with respect to ice (RH_{ice}) and water vapor mixing ratio (H_2O). However, though airborne ~~in-situ~~ in situ measurements best represent detailed microphysical properties of cirrus and their environment, they are always snapshots of specific situations that are also limited by the possibilities of the flight patterns and thus not suitable to derive spatial geographical or seasonal views of cirrus clouds. For this purpose, a globally complete dataset of remote sensing observations from satellite observations are the better option. Hence, as a next step of the study we use ~~in-situ~~ in situ climatologies to evaluate cirrus N_{ice} from satellite observations and, based on this, derive a global

[1] mean mass radius $R_{ice} = \left(\frac{3 \cdot IWC}{4\pi\rho \cdot N_{ice}}\right)^{1/3}$ with ρ= 0.92 g/cm^3

climatology of cirrus N_{ice}. From the portrayal of the two Cirrus Guide II data sets emerging from this study together with some more detailed analyses, we show that the combined evaluation of airborne ~~in-situ~~ in situ and satellite remote sensing observations enhances the insights ~~in~~ into cirrus properties. The ~~in-situ~~ in situ observations are best suitable for the investigation of specific, smaller scale phenomena and for the evaluation of satellite observations or model simulations. Satellite-borne observations, on the other hand, allow a view of the larger scale and seasonal properties.

The article is structured as follows: The Cirrus Guide II ~~in-situ data bases and the used methods~~ in situ databases and the methods used are described in Section 2 and Appendix A. As an overview, in Section 3 we portray the ~~in-situ~~ in situ cirrus cloud and humidity ~~data base~~ database with respect to altitude for the latitudes covered by the observations. The usefulness of the data set is shown by discussing the characteristics and occurrences of ~~in-situ and liquid origin~~ in situ-origin and liquid-origin cirrus. Section 4 first presents cirrus and humidity climatologies of the extended Cirrus Guide II ~~in-situ~~ in situ data base in terms of temperature in comparison to the earlier studies mentioned above. Further, characteristic properties of mid-latitude and tropical climatologies are presented.

In Section 5 we show another example of a specific analysis extracted from the Cirrus Guide II ~~in-situ~~ in situ data base: the data set includes recent unique measurements in the tropical tropopause layer (TTL) region of the Asian monsoon anticyclone, where cirrus clouds and humidity are of special interest and observations are rare. The topic is briefly introduced before the special observations in the Asian monsoon are presented and compared with the conditions found in the surrounding tropical regions.

The last part of the study (Section 6) is the step to global climatology of cirrus N_{ice} from satellite remote sensing observations. For this purpose, the Cirrus Guide II ~~in-situ data base~~ in situ database is used to evaluate remote sensing cirrus observations. Based on this, a global N_{ice} climatology is derived and first analyses of the global and also regional N_{ice} are presented.

2 ~~Data bases~~Databases

2.1 ~~In-situ~~ in situ data set

The observations presented here include the ice water content IWC, the ice crystal number concentration N_{ice}, the mean mass radius R_{ice} in-cloud as well as the clear sky RH_{ice} and clear sky water vapor volume mixing ratio H_2O. The complete ~~in-situ~~ in situ data set comprises 24 field campaigns: the 17 experiments shown in Part I of this study (Krämer et al., 2016, ; the campaigns were performed between 1999 and 2014 over Europe, Africa, Seychelles, Brazil, Australia, USA and Costa Rica), extended by the field campaigns SPARTICUS 2010 and START 2008 over Central US, LTU

2012-2018 over Kiruna, CONTRAST and ATTREX in 2014 and POSIDON 2016 over the tropical Pacific as well as StratoClim 2017 out of Nepal.

A map of flights during the various campaigns (extended map of Cirrus Guide: Part I) is shown in Figure 1. In the Appendix A, a summary of the field campaigns and deployed instrumentation is given in Table 4; Table 5 lists all campaigns and the measured parameters. Also, a discussion of new data evaluation methods, data quality and data coverage is presented. An overview of each campaign is given in the Supplementary Material (SM in the following). Twenty campaigns are chosen to be included in the climatologies; four campaigns (marked in Table 5), where the data volume is very low (START 2008, LTU 2012-2018) or very massive (SPARTICUS in 2010, CONTRAST 2014), so that their contribution to frequency occurrences is either negligible or dominant, are shown in the overview of measurements only (SM).

The climatologies are advanced in several aspects in comparison to the compilations of IWC by Schiller et al. (2008), Luebke et al. (2013) and Krämer et al. (2016) and N_{ice}, R_{ice} and RH_{ice} by Krämer et al. (2009):

- The number of flights and total time in cirrus increased from 104 flights / 94 hours (Krämer et al., 2016) to a total of 150 flights / 168 hours, i.e. the ~~data base~~ database disporportionally has extended by about a factor of 5-10 depending on the specific parameter.
- For IWC, a new data product has been developed that increases the observed data volume (Appendix A2.1).
- For N_{ice}, observations from advanced and extended instrumentation could be added to the ~~data base~~database; further, a new correction of the occurrence frequencies is applied (Appendix A2.2).
- The geographical spread of the observations has broadened, so that a portrayal of cirrus and humidity with respect to the geographical regions mid-latitude and tropics, and also latitude/altitude seems worthwhile.
- As in the earlier climatologies, all data underwent strict quality control.

2.2 Satellite data set

DARDAR-Nice provides observational-based estimates of N_{ice} obtained from CALIPSO and CloudSat measurements (Sourdeval et al., 2018). This unique approach uses the sensitivity of lidar and radar measurements to small and large particles, respectively, to constrain two parameters of a particle size distribution (PSD) parametrization and N_{ice} is subsequently estimated by direct integration, from a minimum threshold size set in this study to 5 µm. DARDAR-Nice uses the parametrization by (Delanoë et al., 2005), in which two normalization parameters (a slope parameter $N_0^\star$ and the volume-weighted diameter D_m) are used to predict the shape of a PSD. Sourdeval et al. (2018) have

demonstrated that the method of Delanoë et al. (2005) is theoretically capable of predicting N_{ice} from recent ~~in-situ~~ in situ campaigns, by comparing its prediction based on ~~in-situ~~ in situ $N_0^\star$ and D_m measurements to the actual ~~in-situ~~ in situ N_{ice} measurement. Good agreements were found, ~~except for temperatures higher than about -50°C where an overestimation in DARDAR-Nice due to~~ although it was noted that the inability of the modified gamma distribution to match the frequently bi-modal shape of the measured PSDs could lead to an overestimation of Ni in DARDAR-Nice. This typically occurs at temperature above -50°C and is expected to be cloud-type dependent, but Sourdeval et al (2018) showed that Ni still was in reasonable agreement with the in situ (a factor of 2) down to T = -30°C, which should cover the entire cirrus temperature ranges in this study.

This evaluation framework is here repeated on the basis of 5 ~~in-situ~~ in situ campaigns archived in the Cirrus Guide II ~~in-situ data base~~in situ database: COALESC2011, ACRIDICON2014, AT-TREX2014, MLCIRRUS2014, STRATOCLIM2017. Based on the agreement between DARDAR-Nice and the ~~in-situ~~ in situ observations, a global N_{ice} climatology is derived from 10 years of satellite observations. Regional N_{ice} climatologies for the Arctic (90N - 67.7N), Northern mid-latitudes (67.7N-23.3N), Tropics (23.3N - 23.3S), Southern mid-latitudes (23.3S - 67.7S) and Antarctica (67.7S - 90S) are analysed in more detail. The results are presented in Section 6.

3 Vertical distribution of cirrus and humidity from in situ observations

As an introduction, atmospheric temperature profiles in the Arctic, at mid-latitudes and in the tropic are shown in Figure 2, (left panel, adopted from Schiller et al., 2008). Exemplarily, vertical profiles inside of cirrus clouds are shown for 28 flights, using blueish colors for Arctic, greenish for mid-latitude and reddish for tropical observations. It can be seen that in the tropics, with the strongest warming of the Earth's surface by the sun, the air is much warmer at higher altitudes than at mid-latitudes or in the Arctic. The coldest atmospheric temperatures are found at the points where the slopes of the temperature profile reverses: the cold point tropopause (CPT). This is the region where the transition from the troposphere to stratosphere occurs. Above the CPT, in the stratosphere, almost no cirrus clouds are observed because it is too dry for ice formation ~~. This can be seen in the right panel of~~ (Schiller et al., 2009). The relations between temperature as well as altitude and the potential temperature Θ are shown in Figure 2~~,~~, middle and right panel for the different geographical regions. ~~(adapted from Schiller et al., 2009, with annotations), where total (= water vapor + evaporated ice crystals) is plotted versus the potential temperature~~ Θ is often used in upper troposphere–lower stratosphere (UT/LS) research, since it allows a clear assignment of air parcels to the associated atmospheric layer, in contrast to the temperature, whose course reverses above the CPT. [2] The range of the tropical tropopause layer (TTL) and the tropical CPT are marked by magenta lines (after Fueglistaler et al., 2009).

[2] ~~Θ is often used in upper troposphere–lower stratosphere (UT/LS) research, since it allows a clear assignment of air parcels to the associated atmospheric layer, in contrast to the temperature, whose course reverses above the CPT. The relations~~

~~for the tropical field campaign TROOCINOX (Brazil, 2005), color coded by total expressed as relative humidity over ice (). Data points right of the clear sky represent a few overshooting convective tropical cirrus clouds (see Section 5) , where the total water is enhanced by evaporating ice crystals. In clear sky conditions above the CPT, is very low and the air is correspondingly dry. Below the CPT , together with humidity are rapidly increasing with decreasing .~~

3.1 Latitude - altitude distributions

As ~~first portrayal~~ a first application of the Cirrus Guide II data set the distribution of cirrus clouds and humidity is shown with respect to latitude and altitude in Figure 3. Plotted are IWC (color coded by volume mixing ratio), N_{ice} (color coded by concentration), R_{ice} (color coded by size), in-cloud as well as the clear sky humidity (color coded by RH_{ice}) and H_2O (color coded by volume mixing ratio). The color codes range from yellow to blue with increasing amount of the respective parameter; note that the data points are plotted in the order of the colors from yellow to blue. The data were collected in the latitude range from about 70°North to around 20°South, i.e. the northern mid-latitudes and the tropics are covered by the observations. The altitude range is between about 5 to 20km. The times of data sampling are displayed in the respective panels; a more detailed description of the ~~data base~~ database is given in Section 4. The way the data is presented here as individual points was chosen because the entire range of measurements is visible. Although data overlap occurs in this type of display, it is possible to identify cirrus types and microphysical processes, especially based on extreme values. As additional overview information, we have created latitude-altitude intervals (500 m altitude, 0.5° latitude) and calculated the 25, 50 (median) and 75 % percentiles for all variables. These additional altitude-latitude climatologies are shown in the SM (Figures 1–3).

Cirrus clouds are found at lower altitudes at mid-latitudes and reach higher levels in the tropical region (Figure 2). Though this structure in the measurements is influenced by the maximum or minimum height the engaged aircraft can reach, it corresponds well with the CALIPSO latitudinal height distribution of cirrus clouds, which is largely caused by the decrease in tropopause height with increasing latitude (shown in the review article by Heymsfield et al., 2017a, original figure by Sassen et al. (2008)).

3.1.1 ~~In-situ~~ in situ-origin and ~~liquid origin~~ liquid-origin cirrus

Krämer et al. (2016), Luebke et al. (2016) and Wernli et al. (2016) describe two different cirrus types: (1) ~~in-situ origin~~ in situ-origin cirrus that form (by heterogeneous or homogeneous ice nucleation on ice nucleating particles, INP, or soluble solution aerosol particles, respectively) from water vapor directly as ice at $T < 235K$, $RH_{ice} > 100$ % and $RH_w < 100$ %; (2) ~~liquid origin~~ liquid-origin cirrus that evolve (also heterogeneously or homogeneously) from freezing of liquid drops in clouds

~~between and temperature as well as altitude and are shown in Figure 2, middle left and middle right panelfor the different geographical regions.~~

at T $\gtrsim$ 235K and $RH_w \sim 100$ % [2] . In other words, ~~in-situ origin~~ in situ-origin cirrus are observed at the altitudes where they are formed, whereas ~~liquid origin~~ liquid-origin cirrus are glaciated liquid clouds from further below which are lifted to the cirrus temperature region where liquid water no longer ~~exist~~exists.

Microphysical characteristics: In the ~~following, the~~ new in situ data set, containing advanced measurements and extended by several field campaigns in comparison to the earlier studies, some typical characteristics of the cirrus types ~~are briefly described~~ and hints to ice nucleation mechanisms are visible. In the following, the cirrus types are briefly introduced, and, using Figures 3 and 4, the types and freezing mechanisms are discussed and summarized in ~~tabular form in~~ Table 1.

~~IN-SITU ORIGIN~~IN SITU-ORIGIN cirrus ~~split~~ can be devided in two sub-classes ~~,~~ depending on the strength of the updraft: in *slow updrafts* ~~, in-situ~~ [3] , in situ-origin cirrus form mostly heterogeneously and are rather opitcally thin with lower IWCs and few but large ice crystals. We like to note here that in an atmosphere free of INPs, cirrus clouds ~~appearing~~ forming homogeneously would have similar characteristics, since also only ~~few ice crystals are nucleated homogeneously at~~ a small number of ice crystals nucleate homogeneously in slow updrafts (see e.g. Spreitzer et al., 2017). Hence, in this regime, the freezing process is not relevant for determining the cirrus properties. In *fast updrafts*[3] , homogeneous freezing ~~is mostly triggered~~ mostly occurs regardless of the presence of INPs, since fast updrafts cause RH_{ice} to reach the homogeneous freezing threshold even after ~~heterogenous~~ heterogeneous freezing. The ~~in-situ~~ in situ-origin cirrus that emerge in these situations are optically thicker with higher IWCs and more but smaller ice crystals.

~~LIQUID ORIGIN~~LIQUID-ORIGIN cirrus stem from lower altitudes, where more water is available, so they generally consist predominantly of thicker cirrus with higher IWC, together with more and larger ice crystals that are frozen heterogeneously at T $>$ 235K in *slower updrafts*. In *fast updrafts*, ~~liquid origin~~ liquid-origin cirrus with very high N_{ice} appear. The reason is that in such updrafts RH_w and RH_{ice} are both $>$ 100 % and thus the Wegener-Bergeron-Findeisen process, where liquid drops evaporate and ice crystals remain at $RH_w < 100$ % and $RH_{ice} > 100$ %, is suppressed (Korolev, 2007). Thus, the numerous supercooled drops reach the altitude (temperature $\sim$ 235K) where they freeze homogeneously (Costa et al., 2017).

The meteorological situations where slow updraft ~~in-situ~~ in situ-origin cirrus frequently occur (see Krämer et al., 2016) are low- and high-pressure systems (frontal/synoptic cirrus). The warm conveyor belt in low pressure systems can also produce ~~liquid origin~~ liquid-origin cirrus. Fast updraft ~~in-situ and liquid origin~~ in situ-origin and liquid-origin cirrus occur in ~~-often orographically induced-~~ gravity waves, often orographically induced, in jet streams and in convective systems and anvils.

[2] For a more detailed description of the freezing mechanisms see Vali et al. (2015); Heymsfield et al. (2017a) and references therein.

[3] slow updrafts: $\lesssim$ 10cm/s; fast updrafts: 10 cm/s - 10 m/s (based on simulations of Kärcher and Lohmann, 2002; Krämer et al., 2016)

As outlined in the Cirrus Guide I (Krämer et al., 2016), to a certain extent cirrus types can be identified by their typical characteristics. This applies to the initial stage, after which the clouds lose the signature of the formation process e.g. by sedimentation: as long as an updraft prevails (corresponding $RH_{ice} > 100\%$), smaller ice crystals in the size range $\lesssim$ 20µm grow to larger sizes on a time scale of tens of minutes. The larger ice crystals sediment to lower altitudes, thus removing ice surface from the cloud volume which consequently reduces the depletion of H_2O_{gas} ($\propto RH_{ice}$) by water vapor transport to the ice (for more detail see Spichtinger and Cziczo, 2010). The ice crystals that have fallen out of the layer deepen the cirrus extent to lower altitudes (fall streaks can extend the cirrus to several km below the nucleation level Jensen et al., 2012; Murphy, 2014), while at the same time, large ice crystals from above could sediment into the cloud volume. Altogether, the cirrus evolution is a dynamical process and the cirrus properties change in the course of a cirrus lifetime. At the final cirrus stage, i.e. when the temperature increases, the environment becomes subsaturated ($RH_{ice} < 100\%$) and ice crystals evaporate, disappearing the faster the smaller they are (timescales of growth and evaporation of ice crystals are shown in Kübbeler et al., 2011, their Figure 12).

Cirrus types with the most striking features (high IWC / N_{ice}) are the easiest to identify. They could be ~~liquid or in-situ origin~~ liquid-origin or in situ-origin cirrus in fast updrafts or also ~~liquid origin~~ liquid-origin cirrus in slow updrafts. This will be shown on the basis of Figure 3 and Figure 4.

In Figure 4, the relation between N_{ice}, R_{ice} and IWC is shown for ~87 h of cirrus cloud observations. It can be nicely seen that in ~~case~~ the cases where N_{ice} is high, the ice crystals are small – because the numerous ice crystals consumed all of the available vapor, thereby suppressing further growth – while low N_{ice} are related to large ice crystals for a given IWC. The IWC (in mg/m^3) ~~can be recognized~~ is indicated by the color code and result from the combination of both N_{ice} and R_{ice}. The thin black lines are isolines of IWC (in ppmv) that appear in the order shown the legend. The scheme at the right side illustrates the partitioning of the clouds between liquid and ~~in-situ origin~~in situ-origin: the thickest cirrus (blue points) are of ~~liquid origin~~liquid-origin, the thinnest (yellow points) of ~~in-situ origin~~in situ-origin. As the thickness of the cirrus decreases, the ~~portion of liquid origin~~ fraction contributed by liquid-origin cirrus becomes smaller and smaller while ~~more and more in-situ origin cirrusappear~~an increasing fraction is due to in situ-origin cirrus.

~~So most~~ Most of the highest IWCs (> 10 mg/m^3, dark red and blue diamonds in Figure 3, top left panel) are of ~~liquid origin~~liquid-origin. They appear in the lower parts of the clouds, i.e. they are uplifted from farther below. A good example of this is the field campaign SPARTICUS in 2010, which is separately plotted in ~~Figure 6~~ Figure 7 of the SM (right panel). About 23 hours of sampling in mostly ~~liquid origin~~ liquid-origin clouds were performed over ~~Central~~ central USA. The clouds ~~are recorded~~ were observed in the temperature range 210-240 K, ~~which corresponds~~ corresponding to altitudes between 5-10 km, i.e. they ~~are~~ were rather low cirrus clouds. The IWCs are mostly high (red to blue colors) and, as shown by Muhlbauer et al. (2014), ice particles ~~up to thousand m diameter and more are present in most measurements, which is indicative for liquid origin~~ of greater than a

thousand µm diameter were frequently encountered, indicative of liquid-origin cirrus (see Table 1). In the tropics (Figure 3), some blue points are also detected at high altitudes of about 17 km ~~. They are observed~~ from measurements made above the Asian monsoon in strong convective updrafts (see also Section 5) and consist of many ice crystals (0.1-10 cm^{-3}) with medium R_{ice} (20-70 µm).

Generally, the IWC roughly shows a vertical structure of decreasing IWC with increasing altitude. This is caused on the one hand by the amount of available water that decreases with decreasing temperature, but also because cirrus of ~~liquid origin~~ liquid-origin predominate in lower layers, whereas cirrus with ~~in-situ origin~~ in situ-origin become more abundant at higher altitudes, i.e. colder temperatures. This is in accordance with the findings of Luebke et al. (2016); Wernli et al. (2016) and Wolf et al. (2018), where Luebke et al. (2016) and Wolf et al. (2018) experimentally investigated the two cloud types in mid-latitudes and in the Arctic, respectively, while Wernli et al. (2016) analyzed 12 years of ERA-interim data in the North Atlantic region (see also Section 6.2).

As ~~the~~ IWC is an indication for the cirrus type, N_{ice} (Figure 3, middle left panel) ~~can give hints on~~ provide a hint to the freezing mechanism, either heterogeneous or homogeneous: high ice crystal numbers N_{ice} ($\gtrsim$ 0.5 cm^{-3}, dark red and blue diamonds, middle left panel of Figure 3) are an indicator for homogeneous ice formation in fast updrafts caused by waves or convection, both for ~~in-situ~~ in situ-origin as well as for ~~liquid origin~~ liquid-origin cirrus. At mid-latitudes, they are found e.g. at the tops of mountain wave clouds (the ice nucleation zone), which were observed for example behind the Norwegian mountains at around 62°North. High N_{ice} values have also been observed in tropical deep convection around 10°North, corresponding to measurements reported by Jensen et al. (2009).

Another source of mid-latitude high N_{ice} are young contrails. Note however, that these high N_{ice} ~~are transient, that means they do not exist for a long~~ exist only for a short time. This is because high ice crystal numbers are associated with small ice crystal sizes (~~blue~~ yellow diamonds in the bottom left panel, see also Figure 4) that grow/evaporate quickly. At lower altitudes, N_{ice} tends to be lower and the crystals are larger, because large crystals having lower concentrations sediment out from the cloud tops and, as mentioned above, ~~liquid origin~~ liquid-origin cirrus with characteristic large ice crystals are also common in this altitude range. In the tropics, high N_{ice} at high altitudes are induced by ~~in-situ~~ in situ homogeneous freezing in convection or gravity waves ~~(see alo Jensen et al., 2013a)~~(see also Jensen et al., 2013a). At cloud bases, such high N_{ice} are most probably of ~~liquid origin~~liquid-origin, initiated by homogeneous freezing of supercooled drops.

A more detailed discussion of the microphysical properties of cirrus including frequencies of occurrence of specific signatures which can not be seen from Figure 3, is given in Section 4.

Radiative characteristics: A motivation to study cirrus clouds is to investigate the ~~radiation~~ radiative properties on the basis of the findings on their microphysical properties. In the Cirrus Guide I, Krämer et al. (2016) speculated that the physically and optically thinner in situ slow updraft cirrus cause a warming effect, while ~~the thicker in situ fast updraft and particularly the thick liquid~~

~~origin~~ thicker fast updraft in situ-origin and, particularly, thick liquid-origin cirrus have the potential to cool. Here, we show a first estimate of the radiative forcing of typical ~~in-situ~~ in situ-origin slow and fast updraft as well as ~~liquid origin~~ liquid-origin cirrus (Figure 5). To this end, radiative transfer calculations for idealized scenarios under specific conditions are realized, at noon at the equinox, which are briefly described in the caption of Figure 5.

In the left panel of ~~the Figure~~Figure 5, the radiative forcing of the slow (light green) and fast (dark green) ~~in-situ origin~~ in situ-origin cirrus is displayed with respect to ~~the~~ optical depth. This panel is ~~zoomed into~~ expanded from the right panel, where the forcing of the ~~liquid origin~~ liquid-origin cirrus is shown. Obviously, the net radiative forcing of the ~~in-situ origin~~ in situ-origin cirrus is much smaller than that of ~~liquid origin~~ liquid-origin and, moreover, change the sign from warming to cooling.

In more detail, the slow ~~in-situ origin~~ in situ-origin cirrus have only small optical depth (τ) between 0.001 - 0.05, resulting in a slight net warming effect of not larger than about 1.5 W/m^2. The optical depth of fast ~~in-situ origin~~ in situ-origin cirrus is larger (τ: 0.05 - 1), but most of them are also warming (2-10 W/m^2). ~~However, the thickest fast in-situ origin~~ The thickest fast-updraft in situ-origin cirrus at the lowest altitudes change the sign of their net forcing, they switch to a slight cooling effect. The reason is the warmer temperature at lower altitude that reduces the warming effect of the longwave infrared radiation. The ~~liquid origin cirrus~~ results of the radiative forcing calculations for the slow and fast updraft cirrus are in agreement with investigations from lidar observations reported by Kienast-Sjögren et al. (2016) and Campbell et al. (2016), who observed cirrus with optical depth up to 1 and 3, respectively, and found a decreasing warming effect with decreasing optical depth. Campbell et al. (2016) even reported a slight cooling effect at the warmest observed cirrus. The liquid-origin cirrus, however, mostly found in the warmest cirrus layers, have large optical depths (τ: 1 - 12), which is larger than the range of cirrus optical depth reported in many studies ~~(the maximum optical depth is often assumed as 3, e.g. Sassen et al., 2008; Mitchell et al., 2018, ; note that this is likely bec~~ (the maximum optical depth is often found to be 1-3, e.g. Sassen et al., 2008; Kienast-Sjögren et al., 2016; Campbell et al., 2016; M . A consequence of the large optical thickness is a quite strong net cooling effect (- 15 to -250 W/m^2) of ~~liquid origin~~ liquid-origin cirrus. These values are of the same order of magnitude as reported from direct measurements inside of cirrus clouds (Wendisch et al., 2007; Joos, 2019).

Thus, from this first and very idealized simulations, we can conclude that ~~in-situ~~ in situ formed cirrus clouds are most likely warm the atmosphere, whereas ~~liquid origin~~ liquid-origin ice clouds have the potential for strong cooling. Note here, that we only investigate local time 12 h, where the cooling is probably most pronounced. For lower sun position (i.e. larger zenith angle) the cooling is probably reduced and during night time, cirrus clouds can only warm the atmosphere (due to the thermal greenhouse effect). Thus, the net effect of cirrus clouds averaged over the whole daily cycle is not yet clear. Such investigations go beyond the scope of this study and are subject of future work.

3.1.2 Humidity

The distribution of in-cloud and clear sky RH_{ice} as well as water vapor H_2O with latitude and altitude is shown in the right column of Figure 3. It can nicely be seen how the amount of H_2O decreases with altitude (bottom panel). The clear sky RH_{ice} (middle panel) ranges from very dry conditions ($< 70\%$ green and orange diamonds) up to highly supersaturated regions ($> 130\%$, dark red and blue diamonds), which mainly are found at high altitudes in the tropics. Such high supersaturations are also found inside of the tropical cirrus clouds (top panel). The behavior of RH_{ice} will be further discussed in Sections 4 and 5.

4 ~~In-situ~~ In situ climatologies

With the term climatologies we refer here to statistical evaluations of the available variables with regard to temperature or potential temperature.

4.1 The IWC-T parameter space: median N_{ice}, R_{ice}, RH_{ice}

In the Cirrus Guide I (Krämer et al., 2016), observations and model simulations are portrayed in the Ice Water Content- Temperature (IWC-T) parameter space. One result of the simulations is that IWC and N_{ice} are correlated with each other. This relationship has been confirmed for some meteorological situations by examples from six individual field campaigns. The database of combined IWC-N_{ice} measurements has grown considerably since then, and with it the covered temperature range of the observations. In the Cirrus Guide I, only few observations below 200 K were available.

With the extended Cirrus Guide II data set, we further investigate the appearance of N_{ice}, but also the corresponding mean mass size R_{ice} and the in-cloud RH_{ice} in the IWC-T parameter space. In Figure 6, medians of the respective parameters are presented in intervals (five iwc intervals per order of magnitude, 1K temperature intervals) covering the entire IWC-T parameter space. The variability of the parameters can be seen in Figures 1–3 of the SM, where the 25, 50 (median) and 75 % percentiles for the variables are shown.

4.1.1 IWC-T-N_{ice} and R_{ice} relation

Observational evidence for the correlation between IWC and N_{ice} can nicely be seen in the upper panel of Figure 6. Almost symmetrical colored bands of N_{ice} can be seen across the entire IWC-T parameter space (N_{ice} concentration increases from yellow to blue). With decreasing temperature, the same N_{ice} numbers cause lower IWC values, which is caused by the likewise decreasing available water content of the air. This finding might be of importance for parametrizations used in global models or satellite retrieval algorithms, where IWC is often the only available parameter that characterizes cirrus clouds, but functions are used to assign N_{ice} to specific IWCs. This new analysis can be used

(after some smoothing of the bands, which will be subject of a follow up study) as lookup table to derive N_{ice} from the information of temperture and IWC.

The ice crystal sizes also form colored bands in the IWC-T parameter space (Figure 6, middle panel; R_{ice} inreases from yellow to blue, running diagonally through the IWC-T room with the size of the ice crystals increasing with increasing temperature (and thus decreasing amount of available water). This is because R_{ice} is calculated from the third root of the IWC divided by N_{ice}, as described in Section 1. However, the R_{ice} bands are somewhat less clear delineated from each other than the N_{ice} bands. They might be smoothed in the follow up study, so that R_{ice} can also be assigned to the IWC-T data points.

One could have expected to find distinct pattern for in situ-origin and liquid-origin cirrus in this type of analysis to quantify the characteristics of the cirrus types shown in Table 1. However, the differences are merged by the calculation of median values in the overlap regions of the types in the IWC-T parameter space. However, we believe that the more heterogeneous structure of the R_{ice} bands is caused by the different cirrus types, because the ice crystal size is their most pronounced difference. A longer term research goal is to derive the IWC-T-N_{ice}-R_{ice} relations seperately for in situ-origin and liquid-origin cirrus.

4.1.2 IWC-T-RH_{ice} relation

In the bottom panel of Figure 6, median in-cloud RH_{ice} are shown in the IWC-T parameter space. Also for RH_{ice} pattern are visible: RH_{ice} decreases with decreasing IWC. Above the median IWC (black solid line), RH_{ice} is mostly between 90-110 % (orange data points), i.e. around saturation. This corresponds to the existence phase of the cirrus (between 110-100 / 100-90 %, the ice crystals slowly grow /evaporate). Below the median IWC, the median RH_{ice} decrease with decreasing IWC (green and yellow data points), reflecting the evaporation phase of the cirrus clouds. Interesting is the distribution of the higher supersaturations (red and blue points): at low temperatures, the clouds tend to higher supersaturations. This has been discussed by (Krämer et al., 2009) for thin cirrus (low IWC) and explained by the corresponding low N_{ice}, whose small ice surface cannot efficiently deplete the water vapor. However, the supersaturations are also seen at high IWC ($\sim$ high N_{ice}). The reason for that is the vertical velocity, which is -together with the ice surface and temperature- a driver of the RH_{ice} ($RH_{ice} = H_2O/H_2O_{sat,ice}(T)$). The air inside of clouds is supersaturated in cases the depletion of H_2O on the available ice surface (decrease of RH_{ice}) cannot compensate for the increase of RH_{ice} caused by the cooling of the air (decrease of $H_2O_{sat,ice}(T)$ with decreasing temperature). High IWC, coinciding always with high N_{ice}, appear in high updrafts, in in situ-origin as well as in liquid-origin cirrus. These high updrafts allow that the supersaturations remain high despite the large ice surfaces available for deposition of excess water vapour. This was also reported by Petzold et al. (2017), who observed high RH_{ice} together with high N_{ice} in tropical convective cirrus on board of passenger aircraft (IAGOS).

4.2 Entire in situ climatologies

The Cirrus Guide II data set shown in Figure 3 is now displayed as frequencies of occurrence ~~in dependence on~~ as a function of temperature (binned in 1 K intervals, Figure 7) and discussed in comparison to the earlier ~~in-situ~~ in situ climatologies presented by Schiller et al. (2008), Krämer et al. (2009) and Luebke et al. (2013) (~~Figure ??).~~ Figure 6, SM). Further, as mentioned above, the new data set is large enough to split it in mid-latitude and tropical cirrus. The differing cirrus cloud properties are presented in Figures 8 and the respective clear sky and in-cloud RH_{ice} in Figures 9.

4.3 ~~Entire in-situ climatologies~~

4.2.1 Ice water content (IWC-T)

Figure 7 (top left panel) depicts the IWC. The black solid and dotted lines represent the median, minimum and maximum IWC of the core IWC band, that is the envelope of the most frequent IWC (>5% per IWC-T bin, Schiller et al., 2008).

The number of hours ~~spend~~ spent sampling in cirrus clouds ~~raised~~ increased from 27 hours in Schiller et al. (2008), 38 hours in Luebke et al. (2013) and 94 hours in (Krämer et al., 2016) to 168 hours in the new extended data set. Part of the additional data is due to the new IWC data product that is applied to all campaigns and combines the IWC from total water measurements as well as the IWC derived from cloud particle size distributions (see Appendix A2.1).

However, the median IWC and the core IWC band -decreasing with temperature as described by Schiller et al. (2008)- is still valid, showing that the IWC measurement techniques are robust and that the IWC is a stable parameter describing cirrus clouds. Note here that ~~below about~~ at temperatures $\lesssim$ 200 K data points ~~below~~ underneath the lower dotted line are not unambiguously identified as clouds, while above about 200 K this threshold is 0.05 ppmv. For more detail see also Appendix A2.1.

4.2.2 Ice crystal number (N_{ice}-T)

About 90 hours of N_{ice} observations are shown in Figure 7 (middle left panel [4]), which is an increase of about a factor of ten in comparison to the data set of Krämer et al. (2009), who ~~complied~~ compiled 8.5 hours (~~Figure ??~~Figure 6, SM). For N_{ice}, the picture has greatly changed when comparing the old and the new data sets. This is on the one hand due to an extension of the lower detection limit of N_{ice} from $4 \cdot 10^{-3}$ to 10^{-4} cm^{-3} (see Appendix A2.2), but also because the new data set represents a better mixture of different meteorological situations. For example, the higher N_{ice} at warmer temperatures in the Krämer et al. (2009) data set (~~Figure ??~~Figure 6, SM) were caused by flights where lee wave cirrus behind the Norwegian mountains were probed (see also Figure 3, blue diamonds at around 60°North). Also, at temperatures colder than about 200 K, N_{ice} was most often very low. Further,

[4] Note that for N_{ice} -and thus R_{ice}- the number of hours spent in clouds in Figure 7 is less than in Figure 3. For details see figure caption.

the enhanced occurrence frequencies at the lowest concentrations seen in the earlier data set are corrected in the new data evaluation procedures (Figures 17 and ~~??~~Figure 6, SM, middle left panel).

90 hours of aircraft N_{ice} observations within of cirrus clouds is a tremendous amount when taking into account the necessary effort. However, this is still far from being representative for the distribution of N_{ice} in the atmosphere. We nevertheless calculated 10, 25, 50, 75 and 90% percentiles, which are shown as thin, dotted and solid lines in Figure 7 (middle left panel). Note that the 10 and 90% percentiles enclose the core region of N_{ice}, i.e. the envelope of the most frequent N_{ice} (>5% per N_{ice}-T bin). Fits through these percentiles and the median N_{ice} reveal no temperature dependence of N_{ice} (10%, median and 90% N_{ice}: 0.002, 0.03 and 0.3 cm^{-3}). This is different to the slight decrease with temperature of the minimum, middle and maximum N_{ice} lines shown by Krämer et al. (2009), which was, as discussed above, ~~cause~~ caused by two flights with high N_{ice} at comparatively warm temperatures.

It is a question why the N_{ice} do not increase with decreasing temperature, as would be expected because the homogeneous ice nucleation rate then increases. This has been investigated by Gryspeerdt et al. (2018) based on a 10 year global data set retrieved from satellite observations (DARDAR-N_{ice}, Sourdeval et al., 2018, see also Section 6). Gryspeerdt et al. (2018) analyzed the N_{ice} (>5µm) only at cloud tops and also those throughout the cirrus clouds. From the cloud top analysis, a clear increase of N_{ice} with temperature was obvious, while integrating throughout the cirrus this temperature dependence becomes much weaker, though it is still present. Gryspeerdt et al. (2018) propose that the missing temperature dependence in the ~~in-situ~~ in situ results could be due to a lack of ~~in-situ~~ in situ measurements near the cloud top, where the temperature dependence is strongest. Another reason could be that the higher N_{ice} are short-lived (see Section 3.1.1) and thus not easy to trace by aircraft.

A further consideration of N_{ice} frequencies of occurrence on a global as well as regional scales derived from satellite remote sensing will be presented in Section 6.

4.2.3 Ice crystal mean mass radius (R_{ice}-T)

The ice crystal mean size is calculated as mean mass radius R_{ice} as shown in Footnote 1. R_{ice} is close to the common effective cloud particle radius R_{eff} ($\sim$ ice Volume/Area), but can be calculated without knowing details of the ice particle size distribution (see also Krämer et al., 2016).

A total of 84 hours of observations are compiled in Figure 7 (bottom left panel). Overall, the mean mass R_{ice} ranges from about 1 to 100 µm, while individual ice crystals in cirrus can reach sizes up to 1000 µm or even larger. The R_{ice} core band (frequencies $\gtrsim$ 5% per R_{ice}-T bin) decreases slightly ~~with decreasing temperature~~ as the temperature decreases, which is caused by the decrease of the IWC core band, since the N_{ice} band is not dependent on temperature (see previous section).

The 10, 25, 50, 75 and 90% percentiles of the data set are plotted as thin, dotted and solid red lines. The black lines represent the minimum, middle and maximum R_{ice} shown by Krämer et al. (2009) (see ~~Figure ??~~Figure 6, SM). The range of R_{ice} has shifted slightly to larger sizes in the new data

set, which is caused by the N_{ice} range extended towards lower concentrations that mainly consist of larger ice crystals.

Remarkable is the drop of the most frequent R_{ice} from larger to smaller ice crystals seen at around 215 K. This is probably the approximate temperature up to which ~~liquid origin~~ liquid-origin clouds are detected (see Luebke et al., 2016; Sourdeval et al., 2018, and also Section 6.2), that are characterized by larger ice crystals than ~~in-situ~~ in situ-origin cirrus (Krämer et al., 2016). At higher temperatures where both liquid and ~~in-situ origin~~ in situ-origin cirrus prevail, higher IWCs - and thus also a larger R_{ice} - occur more often than at lower temperature where only the thinner ~~in-situ origin~~ in situ-origin clouds exist. This is especially true at mid-latitudes, in the tropics the ~~liquid origin~~ liquid-origin cirrus reach also lower temperatures and thus no sudden drop of R_{ice} is observed (see Figure 8, left and right bottom panel). The bifurcated structure of the most frequent R_{ice} which ~~ca~~ can be seen for temperatures $\lesssim 190$ K is discussed in Section 4.3.1 (vii).

4.2.4 Clear sky and in-cloud RH_{ice} (RH_{ice}-T)

The new RH_{ice} clear sky and in-cloud data sets are displayed in the middle and top right panel of Figure 7. The respective earlier data sets of Krämer et al. (2009) are shown in ~~Figure ??~~Figure 6, SM. The overall picture of the RH_{ice} distributions has not changed substantially, though the amount of in-cloud data ~~base~~ in the database has increased from 10 hours of measurements to about ~~116~~96 hours, and the clear sky observation time from 16 to ~~even 320~~186 hours. The only ~~slight change~~ small difference is found in the in-cloud RH_{ice}, ~~maybe~~ potentially caused by the larger ~~number~~ amount of data: below about 200 K, where high supersaturations (>120%) occur more often and low subsaturations (<80%) less often. At higher temperatures, the peak of RH_{ice} frequencies at 100% is more pronounced.

For the new data set, ~~we show for information~~ in addition to the clear sky RH_{ice} ~~also~~ the absolute water vapor volume mixing ratio H_2O in the bottom right panel of Figure 7 is plotted. To guide the eye, water vapor saturation wrt ice, $H_2O_{sat,ice}$, is drawn as black solid line. The decrease of H_2O with temperature is nicely seen in this panel and clear sky supersaturations appear in this portrayal as data points above $H_2O_{sat,ice}$.

4.3 Mid-latitudes and tropics

4.3.1 Mid-latitude and tropical cirrus clouds

The data sets of mid-latitude/tropical cirrus consist of 67/101 hours of IWC, 29/61 hours of N_{ice} and 28/56 hours of R_{ice} measurements. This section describes some of ~~some~~ the pronounced characteristics of mid-latitudes and tropical cirrus, which are displayed in Figure 8 (greenish/ reddish colors represent mid-latitude/tropical cirrus).

(i) *Temperature ranges:* Comparing mid-latitude and tropical cirrus, the first obvious difference -as expected when looking at the temperature profiles in Figure 2- is the temperature range. The observed mid-latitude cirrus rarely occur below 200 K, while tropical cirrus are detected down to temperatures of 182 K. The core IWC/N_{ice}/R_{ice} range of both mid-latitude and tropical cirrus corresponds to the total climatology (see Figure 7).

(ii) *Mid-latitude WCBs and MCS:* At European mid-latitudes, the most frequent cirrus can be assigned to slow updrafts in frontal systems (WCBs: warm conveyor belts) containing both ~~liquid and in-situ origin~~ liquid-origin and in situ-origin cirrus. High IWCs stem mostly from ~~liquid origin~~ liquid-origin WCB cirrus. Above the ~~US continent~~central USA, mesoscale convective systems (MCS) with faster updrafts are more frequent. The resulting ~~liquid origin~~ liquid-origin cirrus are thicker than the European, i.e. the ice crystals are larger and the IWC is higher (see also Krämer et al., 2016).

(iii) *Contrails:* A striking feature in the cirrus observations are N_{ice} of up to several hundreds per cm^3, that are found at mid-latitudes in the temperature range of about 210-220 K, which corresponds to about 10 km altitude (see Figure 2), the typical cruising level of passenger aircraft. They can be attributed to young contrails, which were a topic of investigation during COALESC 2011 (Jones et al., 2012) and also ML-CIRRUS 2014 (Voigt et al., 2017). Higher mid-latitude N_{ice} at higher temperatures are most probably ~~in-situ origin~~ in situ-origin cirrus caused by stronger updrafts in e.g. mountain waves.

(iv) *Drop freezing:* High N_{ice} between ten and ~~hundredper~~ hundred per cm^3 or even more are found above 235 K. Such high concentrations together with small R_{ice} are typical for ~~frozen supercooled liquid drops, i.e.~~supercooled liquid cloud drops that might be frozen by spontaneous homogeneous drop freezing (that occurs latest at around 235 K in the atmosphere) or not. In any case, these cloud particles are an indication for ~~liquid origin cirrus caused by homogeneous drop freezing~~ liquid-origin clouds caused in tropical or mid-latitude convective systems with fast updrafts.

(v) *Tropical convection:* ~~However~~In contrast, in tropical cirrus, ~~in particular~~ and particularly for temperatures $\gtrsim$ 220 K, high IWCs and N_{ice} above the core range -corresponding to convective ~~liquid origin~~ liquid-origin cirrus- become more frequent, while R_{ice} tends to be smaller. This is most likely caused by the fast convective vertical velocities that often let clouds in the mixed-phase temperature regime rise to the cirrus altitude range.

(vi) *Tropical deep convection:* Also remarkable is that in the tropics, massive convective ~~liquid origin~~ liquid-origin cirrus carrying a high IWC -often accompanied by high N_{ice}- are detected down to very cold temperatures (< 200 K), which corresponds to high altitudes up to 17 km. The thickest cirrus with very high IWC and N_{ice} can also be seen in Figure 3 (upper and middle left panel: distribution of cirrus with latitude; blue data points represent ~~liquid origin~~ liquid-origin with a high IWC/N_{ice}) at around 25° northern latitude and 16-18 km altitude. These exceptional thick and cold cirrus at high altitudes were observed in the Asian monsoon tropical tropopause layer (TTL). The

observed many small N_{ice} are generated most likely by ~~in-situ~~ in situ homogeneous ice nucleation, triggered either by fast updrafts in gravity waves (see also Spichtinger and Krämer, 2013; Jensen et al., 2017) or deep convection. They often occur in the tops of to massive ~~liquid origin~~ liquid-origin cirrus with very high IWC; a theoretical description of such clouds is given by Jensen and Ackerman (2006).

(vii) *TTL cirrus:* The discussion of cirrus clouds in the tropical tropopause layer is presented in Section 5.

4.3.2 Mid-latitude and tropical humidity

The mid-latitude/tropical humidity data sets include ~~35~~24/~~81~~72 hours of in-cloud RH_{ice} and ~~94~~51/~~226~~132 hours of clear sky RH_{ice}/H_2O measurements, which are displayed in Figure 9 with the same color code as in Figure 8.

In clear sky at temperatures higher than about 200 K, RH_{ice} is most often below saturation and randomly distributed in both mid-latitudes and tropics (Figure 9, middle row). Clear sky supersaturations occurs less frequently, simply because they only take place in those periods when moist air parcels are cooled towards the ice nucleation thresholds (heterogeneous or homogeneous), which are rare compared to drier conditions of the atmosphere.

Below about 200 K, i.e. in the TTL (see also Section 5), the clear sky RH_{ice} distribution looks very different. In this region, H_2O is low and its variability is only small (Figure 9, bottom row). We plotted lines of constant H_2O (1.5, 3 and 5 ppmv) in the clear sky RH_{ice} panels to illustrate that for constant H_2O, RH_{ice} increases only due to the decrease in temperature, i.e. $H_2O_{sat,ice}$. Thus it can be seen that at mid-latitudes RH_{ice} mostly represent H_2O values around 3 ppmv and in the tropics between 1.5 and 3 ppmv. Since in the tropics much colder temperatures are reached, the respective RH_{ice} ranges from 10 up to about 150% or even more.

Clear sky RH_{ice} above the homogeneous freezing line are under discussion, because they would indicate that no supercooled liquid aerosol particles are present to initiate freezing, or that the homogeneous freezing is prevented, for example by organic material contained in the aerosol particles. More probably, these few data points are outliers; note also that the uncertainty of RH_{ice} rises from approximately 10% at warmer temperatures to about 20% at colder temperatures (Krämer et al., 2009).

Inside of cirrus, the peak of the RH_{ice} frequencies is mostly around the thermodynamical equilibrium value of 100% (saturation) at mid-latitudes as well as in the tropics (Figure 9, upper row). However, in the TTL, at the coldest prevailing temperatures ($\lesssim$ 190 K), supersaturation increasingly becomes the most common condition, which is discussed in more detail in Section 5. High supersaturations at low temperatures were also reported by (Krämer et al., 2009) and Jensen et al. (2013a), and the reason given for the existence of such high supersaturation is low N_{ice} concentrations, which

were mostly present at low temperatures in these observations (~~Figure ??~~Figure 6, SM). But, Jensen et al. (2013a) also showed that RH_{ice} rapidly drops to saturation in the presence of many ice crystals. As can be seen from Figure 8, middle right panel (and discussed in Section 4.2.2), in the new data set N_{ice} cover a broader concentration range in comparison to the earlier data (~~Figure ??~~Figure 6, SM), while RH_{ice} is supersaturated in most cases. This is not straightforward ~~understandable because of~~ to understand due to the complex relation between RH_{ice} and N_{ice}. We will investigate the TTL supersaturations ~~at~~ in cirrus clouds in a follow-up study.

5 TTL ~~in-situ~~ in situ climatologies in- and outside of the Asian monsoon anticyclone

The tropical tropopause layer is the region above the upper level of main convective outflow, where the transition from the troposphere to stratosphere occurs. It is placed at temperatures <205 K between ∼150 hPa/355 K potential temperature/14 km and 70 hPa/425 K/18.5 km (Fueglistaler et al., 2009, see also Figure 2). The coldest temperatures are found here at the point where the slope of the temperature profile reverses (cold point tropopause, CPT). In the TTL, the prevailing dynamical conditions are very slow large-scale updrafts superimposed by a spectrum of high-frequency gravity waves (i.e. Spichtinger and Krämer, 2013; Dinh et al., 2015; Jensen et al., 2017; Podglajen et al., 2017). In addition, deep convection with fast updrafts ~~can~~ that occasionally overshoot into the TTL~~occasionally~~.

Cirrus clouds and humidity in the TTL deserve a special consideration, because this region represents the main pathway by which water vapor enters the upper troposphere and lower stratosphere (UT/LS) where it is further distributed over long distances (e.g. Brewer, 1949; Rolf et al., 2018; Vogel et al., 2016; Ploeger et al., 2013). This is of importance, because water vapor is a greenhouse gas that has a significant impact on the ~~surface climateof the Earth, especially~~ climate, with greatest sensitivity in the tropical UT/LS (Solomon et al., 2010; Riese et al., 2012), but also in the LS at high latitudes where it is being transported from the tropics. Cirrus clouds are of particular relevance as regulators of the partitioning of H_2O between gas and ice phase. Furthermore, they have a climate feedback themselves by influencing the Earth's radiation balance (e.g. Boucher et al., 2013). Thus, the simultaneous observation and analysis of both cirrus clouds and humidity (H_2O) in this climatically crucial region are of special interest.

This section specifically reports cirrus clouds together with humidity (from the climatologies presented in Section 4), that was recently observed for the first time in the TTL in the Asian monsoon anticyclone (June to September) in comparison to observations in the surrounding tropical regions. As the Asian monsoon is characterized by strong convective activity, this comparison will show the difference to less active, calmer areas. Observations of Asian monsoon TTL cirrus clouds and humidity are of particular importance because, amongst other trace species, large amounts of H_2O

and also cloud particles are convectively transported upwards from far below, where the additional H_2O in turn often cause cirrus formation (e.g. Ueyama et al., 2018, and references therein). Directly injected H_2O or H_2O from sublimated ice crystals can then be mixed up into the stratosphere. Thus, the Asian monsoon anticyclone represents ~~the major~~ a significant gateway for H_2O between UT and LS (e.g. Fueglistaler et al., 2009; Ploeger et al., 2013) and currently it is under discussion to what extent cirrus cloud particles contribute to the amount of H_2O entering the stratosphere (e.g. Ueyama et al., 2018, and references therein).

The airborne measurements in the Asian monsoon (see Figure 1 and Tables 4 and 5) ~~are~~ were performed during July-August 2017 out of Khatmandu, Nepal, during a field campaign embedded in the StratoClim project (http://www.stratoclim.org/). An overview of the observations is given in Figures 10, 11 and 12, where the frequencies of IWC, N_{ice}, R_{ice} and in-cloud, clear sky RH_{ice} as well as the clear sky H_2O volume mixing ratio are shown in the temperature and also the potential temperature Θ parameter space. [5] Most of the measurements during StratoClim are performed at temperatures $\lesssim$205 K, corresponding to potential temperatures $\gtrsim$355 K and altitudes about $\gtrsim$14 km, i.e. in the TTL (marked in the middle panels of the Figures).

The surrounding, in most (but not all) cases calmer tropical TTL regions are represented by observations during the campaigns shown in Figure 1 and listed in Tables 4 and 5. The majority of the data ~~are~~ were sampled during ATTREX_2014 and POSIDON_2016. The TTL measurements in the temperature parameter space are shown in Figures 8 and 9; in these plots, the Asian monsoon observations are included, but since the measurements represent only a small part of all TTL observations, excluding the StratoClim campaign only slightly change the frequency distributions. Thus, the Figures are representative for the TTL outside of the Asian monsoon anticyclone, so we refrain from showing an additional Figure. The measurements in the Θ parameter space (StratoClim excluded) are presented in the left panels of Figures 11 and 12.

5.1 TTL cirrus clouds

5.1.1 Temperature parameter space

In the tropics outside of the Asian monsoon (Figure 8, right column), cirrus IWC and N_{ice} range from very low to quite high values. We want to draw attention to a special feature of the most frequently occurring cirrus N_{ice} (middle right column). Two main branches of most frequent N_{ice} are found, one at very low ($\sim 10^{-3}$ cm^{-3}) and the other at moderate ($\sim 5{\cdot}10^{-2}$ cm^{-3}) N_{ice}. These two branches are also reflected in R_{ice}, where the larger ice crystals are found together with lower concentrations and vice versa, as shown in Figure 4. More precisely, cirrus with $N_{ice} \lesssim 1.5{\cdot}10^{-2}$ cm^{-3} consist of ice

[5] The additional Θ portrayal provides a more detailed impression of the distribution of cirrus clouds and humidity around the CPT, i.e. at the transition between troposphere and stratosphere (see Figure 2).

particles larger than about 20 µm [6] . That means that the ice crystal spectra of the low N_{ice} cirrus most likely represent aged clouds (~~in-situ or liquid origin~~in situ-origin or liquid-origin) where the smaller nucleation mode ice crystals are either grown to larger sizes in supersaturations or evaporated in case of subsaturated conditions (see also Section 3.1.1). The middle N_{ice} cirrus containing ice crystals smaller than 20 µm are most likely young cirrus that have formed ~~in-situ~~in situ, because these small crystals quickly (on a time scale of 10 - 20 minutes) grow to larger sizes. It is impossible to speculate if they have formed homo- or heterogeneously, since both pathways might produce such N_{ice} in the slow updrafts prevailing in the TTL. The reason that the aged cirrus marked in Figure 8 (middle right column) become visible only in the TTL, though they certainly occur in all cirrus regions, is probably the calmer dynamic environment with -in comparison to lower altitudes- less frequently occurring temperature fluctuations. These fluctuations likely cause new ice nucleation events ~~superimposing~~ superimposed on the aged cirrus.

The clouds observed in the Asian monsoon include ~~in-situ~~ in situ formed cirrus as well as cirrus clouds from overshooting deep convection. In the much ~~uneasier~~ more convectively unstable Asian monsoon conditions, IWC and N_{ice} are most frequently above the median lines derived from the entire climatology (Figure 10, left column) and also high in comparison to the tropical climatology (Figure 8, right column). Here, the highest observed values (at temperatures $<$205 K) are ~~reached~~ found with IWC mixing ratios of up to 1000 ppmv and a maximum N_{ice} as high as 30 cm^{-3} (note that the ice crystal shattering was significantly minimized, see Section A2.2). Also, the ice crystals mean mass size, R_{ice}, is above the median, especially at very low temperatures, which means that large ice crystals are found around the cold point. These exceptional findings are recorded during flights in strong convection, where ~~liquid origin~~ liquid-origin clouds from far below are detected in the upper part of the Asian monsoon anticyclone simultaneously with freshly homogeneously nucleated ice crystals. The observations were possible due to the pilot of the Geophysica aircraft, who dared to fly into the strong updrafts. Because of the dangerous nature of measurements under such conditions, the frequency of convective – and also orographic wave cirrus – is under-represented in the entire ~~in-situ~~ in situ climatology.

5.1.2 Potential temperature (Θ) parameter space

The distribution of Asian monsoon cirrus clouds in the Θ parameter space ~~are~~ is shown in the right panel of Figure 11. TTL average upper and lower boundaries and the CPT are marked in the middle panel of the Figure following the definition of Fueglistaler et al. (2009). In the left panel of Figure 11, the climatologies of the tropical observations without Asian monsoon are shown.

From Figure 11, upper row, it can be nicely seen how steeply the IWC increases during the transition from the TTL to the free troposphere. In the tropics outside of the Asian monsoon, the

[6] It should be noted that concentrations $\lesssim$0.1 cm^{-3} of cloud particles $\lesssim$20 µm are below the detection limit of cloud spectrometers, i.e. small ice crystals with such low concentrations could be present (see Appendix A2.2).

maximum Θ where ice is detected is about 420 K (∼ 19 km). The mixing ratios of these highest cirrus are about 0.05 ppmv. At about 380 K (CPT, ∼ 16-18 km), the range of most frequent IWCs broadens, ranging between about 0.005 and 1 ppmv. Some higher IWCs are also detected in the upper TTL, indicating that overshooting convection (~~liquid origin~~ liquid-origin cirrus) is also embedded in these measurements. Below about 380 K the most frequent IWC increases steadily up to values of around 10 ppmv at 355 K and 1000 ppmv at 340 K and farther below.

In the Asian monsoon, the maximum Θ where ice is detected is about 415 K (∼0.5 ppmv) and at 400 K the IWC ranges between 0.05 - 0.1 ppmv, as outside of the Asian monsoon. But, at 380 K (CPT), the range of most frequent IWCs rises to 0.5 - 2 ppmv, then steadily increasing below about 380 K to values of around 50 - 500 ppmv at 355 K. Obviously, ~~in~~ IWC near and below the CPT within the Asian monsoon ~~TTL the IWC~~ anticyclone is enhanced by ~~about~~ a factor of ten ~~and more in the Asian monsoon around the CPT and below~~ or more by injection of ~~liquid origin cirrus in convective~~ liquid-origin cirrus in overshooting events. The highest TTL IWCs (up to 1000 ppmv) are detected in the Asian monsoon up to 390 K.

These overshooting cirrus around and below the CPT are also seen in high ice crystal numbers N_{ice} ($\gtrsim$0.5 cm^{-3}) when comparing the Asian monsoon with the other tropical regions (Figure 11 middle panels). Striking are again the high N_{ice} up to 30 cm^{-3} in the Asian monsoon, already discussed with respect to the temperature parameter space. Here it is visible that this burst of ~~in-situ~~ in situ homogeneous ice nucleation in a strong convective event (theoretically described by Jensen and Ackerman, 2006) took place below the CPT.

Above 390 K, at the transition to the stratosphere, N_{ice} is very low, mostly lower than 0.1 cm^{-3}. Recall that these low concentrations only contain particles $>$ 20 µm (Footnote 6 and Appendix A2.2). This means that in the Asian monsoon (middle right panel of Figure 11) low concentrations of larger ice crystals (together wit higher IWCs) are more often present at such altitudes in comparison to the surrounding tropics.

In the TTL outside of the Asian monsoon, the two branches of more frequent N_{ice} (and R_{ice}) – discussed with respect to the temperature parameter space (Figure 8, right middle panel) – are also very clearly visible. The smaller/larger ice crystals with higher/lower concentrations were identified as young and aged cirrus clouds, which most probably have formed ~~in-situ~~in situ. Farther below, N_{ice} further increases with decreasing Θ/altitude and more and more small ~~liquid origin~~ liquid-origin cloud particles (frozen or liquid) with higher concentrations appear.

5.2 TTL humidity

5.2.1 Temperature parameter space

Considering the in-cloud and clear sky RH_{ice} in the Asian monsoon (Figure 10, right column) in comparison to the entire tropical climatologies (Figure 9, right column), significant differences are visible. Below about 200 K, the most frequent in-cloud RH_{ice} are found in supersaturation in the

Asian monsoon cirrus. In the entire climatology (Figure 9, right column) this occurs only below about 185 K. The same is seen in clear sky RH_{ice}: higher supersaturations occur frequently already at higher temperatures in the Asian monsoon comparison to the entire tropical climatology. These higher supersaturations reflect a higher amount of water vapor in the Asian monsoon TTL, visible through the dashed lines in the middle right panel of Figure 10. They show the increase of RH_{ice} caused by the decrease of $H_2O_{sat,ice}$ during cooling of air at a constant H_2O mixing ratio. These lines correspond to H_2O between 3 and 5 ppmv in the Asian monsoon, while in the total tropical climatology the most frequent H_2O ranges only between 1.5 and 3 ppmv (Figure 9; compare also the bottom panels of the Figures, where H_2O is plotted). ~~Inevitably, in case more water is present while cooling of air, supersaturation is achieved~~ Due to the higher water vapor mixing ratios, supersaturation occurs already at higher temperatures. Implications of the observed supersaturations are further discussed in Section 5.3.

5.2.2 Potential temperature (Θ) parameter space

The high RH_{ice} in and outside of cirrus clouds in the Asian monsoon are also visible in the Θ representation of the humidity (see Figure 12, top and middle right panels). In the tropical climatology outside of the Asian monsoon (top left panel of Figure 12), RH_{ice} most frequently center around saturation inside of the cirrus clouds. In the cloud free TTL outside of the Asian monsoon (middle left panel of Figure 12), a humidification of the layer between $\sim$ 360 and 380 K to RH_{ice} around 90% can be seen (for more detail see Schoeberl et al., 2019).

In the Asian monsoon, on the other hand, the in-cloud RH_{ice} in the TTL exceeds saturation (top right panel of Figure 12). Especially, beween 380 and 400 K the most frequent RH_{ice} is around 130%. Also outside of clouds (middle right panel of Figure 12), around the CPT supersaturation is frequently detected and in general the humidification is higher than in the surrounding tropical regions. This is in agreement with Schoeberl et al. (2019), who reported high RH_{ice} coincident with the Himalaya Monsoon during summer and closely associated with convection. The higher amount of water vapor in the Asian monsoon in comparison to the other tropical regions can also be seen in the H_2O volume mixing ratios (bottom panels of Figure 12). In the tropics ~~without~~ outside the Asian monsoon, the most frequent H_2O between 365-410 K is 1.5-4 ppmv, while in the Asian monsoon we found 3-8 ppmv, as also seen in the temperature parameter space. This finding is in accordance to other studies, but has been observed ~~in-situ~~ in situ from aircraft directly in the Asian monsoon for the first time. For example, analyzing the air mass histories of higher ~~in-situ~~ in situ H_2O observations at other locations (highest values of 8 ppmv), Schiller et al. (2009) found that those air masses has passed the Asian monsoon region. Also, Ueyama et al. (2018) (and references therein) reported 5-7 ppmv at 100 hPa from MLS observations and extensive model simulations over the Asian summer monsoon region.

5.3 H_2O and IWC for transport to the stratosphere

The H_2O transport to the stratosphere is regulated by the coldest temperature an air parcel experiences during transition through the tropopause region. The water amount passing the tropopause is set by the freeze-drying process associated with this transition (Jensen and Pfister, 2004) and is discussed to be as low as H_2O saturation at the minimum temperature (e.g. Schiller et al., 2009).

However, Rollins et al. (2016) showed for the ATTREX 2014 observations, that the water vapor at the stratospheric entry point is higher by ∼10%, because the water vapor depletion by ice crystals becomes increasingly inefficient at temperatures below 200 K (note that this is a rough estimate of the excess water vapor at the stratospheric entry point based on the actual temperature, which ~~cloud~~ could be somewhat different from the minimum temperature of the air parcel's back trajectory). This is of importance, since already small amounts of H_2O can influence the stratospheric radiation budget (Solomon et al., 2010; Riese et al., 2012).

High supersaturations at the coldest points of the TTL are also discussed in Section 5.2.1. The ATTREX 2014 and also POSIDON 2016 observations are included in Figure 9, right panels, where the most frequent ~~in cloud and clear~~ in-cloud and clear sky RH_{ice} at these temperatures can be seen to increase with decreasing temperature as discussed by Rollins et al. (2016). But, in the Asian Monsoon measurements (Figure 10, right panels), RH_{ice} at the coldest temperatures is even higher above saturation than in the calmer tropics outside, the saturation is exceeded by about 20-50% below 195 K.

Therefore, we extend the conclusion of Rollins et al. (2016): taking saturation at the stratospheric entry of an air mass as set point for water vapor transport to the stratosphere, the transport is underestimated by ∼10% in regions of weak convective activity. In convective regions the underestimation increased to 20-50% in our observations.

As mentioned earlier, the question of how much H_2O from convectively injected ice crystals is transported from above the CPT further into the lower stratosphere is a subject of recent research. In the study of Ueyama et al. (2018), it is concluded that over the Asian monsoon at 100 hPa, convection is the dominant driver of the localized H_2O and that nearly all of the convective enhancements in H_2O is due to the effect of convective humidification, while convectively detrained ice crystals have negligible impact.

From our measurements in and above the Asian monsoon anticyclone, however, it is difficult to estimate to what extent cirrus cloud particles contribute to the amount of H_2O that might enter the stratosphere. Nevertheless, from Section 5.1 we know that the most frequent IWCs between about 365-400 K are 10 to 0.5 ppmv. Above 400 K, up to 415 K some overshoots with IWCs between 0.5 to 8 ppmv are detected (Figure 11, upper right panel). These IWCs are similar to the amount of gas phase H_2O, which is between 3 to 8 ppmv in this region above the CPT (see last Section). Such

amounts of H_2O and IWC indicate that the air ~~masses originate~~ 'masses originate' from an altitude of about 15 km (Figure 3), which corresponds to the lower bound of the TTL (see Figure 2).

The question is if the ice particles found in the upper TTL will further grow and sediment out in supersaturated conditions (dehydration) or evaporate and add H_2O to the gas phase H_2O in subsaturation (hydration, see Jensen et al., 2007; Schoeberl et al., 2018). Inspecting the in-cloud RH_{ice} (see Figure 12, upper right panel) related to the respective IWCs, it can be seen that the air in the overshoots $\gtrsim$400 K with the fairly high IWCs (0.5 to 8 ppmv) is subsaturated, while at lower altitudes both super- and subsaturation occur. This means that convective overshoots in the Asian monsoon can locally contribute a significant amount of water that might be further transported into the stratosphere. Unfortunately, we can not say anything about the frequency of these events in this study.

Above the CPT in the surrounding tropics outside of the Asian monsoon, the in-cloud RH_{ice} at $\gtrsim$400 K are also subsaturated. Here, the IWCs range only between 0.02 and 2 ppmv, with some single data points up to about 2 ppmv. The related H_2O is 1.5 to 3 ppmv.

Comparing gas phase H_2O and IWC above the Asian monsoon CPT (both 3-8 ppmv) with the surrounding tropical regions (1.5-3/0.02-2 ppmv) might be an indication by ~~in-situ~~ in situ observations that, driven by overshooting convection, the Asian monsoon could by an important source for transport of H_2O to the stratosphere.

6 Global ~~and regional~~ cirrus N_{ice} ~~climatologies~~climatology from satellite remote sensing

Though the new ~~in-situ~~ in situ cirrus climatologies presented in Section 4 represent a considerable data set from research aircraft from which substantial insights are gained, it is still a mixture of different meteorological situations encountered during various field campaigns that does not necessarily display a statistically representative overall picture of the distribution of cirrus cloud properties. For this purpose, long-term global satellite remote sensing observations would be the method of choice, though retrievals of cirrus microphysical properties also have their own difficulties and limitations. This is especially true for the ice crystal number N_{ice}, which is particularly challenging to estimate from satellite remote sensing. The new retrieval method for N_{ice} introduced in Section 2.2, DARDAR-Nice, has however demonstrated ~~to be able~~ the ability to satisfactorily reproduce ~~in-situ~~ in situ ice concentrations (Sourdeval et al., 2018).

In this section, we show a global climatology of N_{ice} derived from DARDAR-Nice in the same presentation as the ~~in-situ~~ in situ N_{ice} climatology. Median N_{ice}, 25/75th and 10/90th percentiles are provided for a global data set. In addition, median N_{ice} are discussed for the Arctic region, the northern mid-latitudes, the tropics, the southern mid-latitudes and Antarctica.

6.1 Comparison of remote sensing and ~~in-situ~~ in situ N_{ice}

As a base for reliable N_{ice} climatologies from satellite remote sensing, ~~in-situ~~ in situ measurements of PSDs (ice particle size distributions) from five campaigns of the Cirrus Guide II are used for an evaluation of the DARDAR-Nice retrieval algorithm (see Section 2.2). This directly follows the evaluation of DARDAR-Nice presented in Sourdeval et al. (2018), ~~where the same campaigns were used.~~ a subset of campaigns from the Cirrus Guide II data set was used. This section therefore focuses on these five campaigns, which are nevertheless representative of a wide range of mid-latitude and tropical ice clouds (see Figure 1 and caption of Figure 13). Figure 13 (top panel) shows the N_{ice} frequencies of occurrence in 1K temperature bins of the ~~in-situ~~ in situ measurements, the corresponding frequencies obtained from DARDAR-Nice are shown in the bottom panel. The latter are derived on the basis of two input parameters which are extracted from the ~~in-situ~~ in situ PSDs of the five campaigns listed in the figure caption, rather than being constrained from lidar-radar measurements during usual retrievals. This approach allows to identify inherent incompatibilities between the satellite retrieval assumptions and the in situ measurements, by assuming that the in situ PSD parameters are perfectly constrained by the lidar-radar. Therefore, possible differences should only be attributed to other retrieval assumptions, such as the PSD shape. Sourdeval et al. (2018) showed that this approach is efficient for identifying algorithmic limitations while still being representative of actual satellite retrievals. Note that DARDAR-Nice provides concentrations of ice crystals $> 5\mu m$, as it has not been evaluated for smaller sizes, while N_{ice} from ~~in-situ~~ in situ observations includes sizes $> 3\mu m$; however, the resulting difference in the ice concentrations is negligible. Also, the 1-Hz ~~in-situ~~ in situ PSDs are here sampled into 10-s averages to simulate the 1.7-km horizontal resolution of the DARDAR-Nice retrievals (assuming a flight speed of about $170\,m\,s^{-1}$).

The black solid and dotted lines of the ~~in-situ~~ in situ climatology indicate the 50, 25 and 75^{th} percentiles, which agree well with those of the entire ~~in-situ~~ in situ climatology (see Figure 7, middle left panel). This demonstrates that the selected subset is statistically representative of the entire database (indeed, the entire N_{ice} climatology contains only one additional campaign, see Table 5). A satisfactory agreement between DARDAR-Nice and the ~~in-situ~~ in situ observations is also seen, demonstrating that DARDAR-Nice N_{ice} retrievals very well match the ~~in-situ data base~~ in situ database for known size distibutions.

A detailed comparison of the DARDAR-Nice percentiles (black solid and dashed lines) with those of the ~~in-situ~~ in situ observations, however, yields a small offset by a factor of 1.73, which is visualized in Figure 13 by the average medians of DARDAR-Nice (straight black line, $0.064\,cm^{-3}$) and ~~in-situ~~ in situ (straight blue line, $0.037\,cm^{-3}$). One reason for this offset lies in the method of the retrieval. The two parameters, $N_0^\star$ and D_m, calculated here from the ~~in-situ~~ in situ PSDs (usually from lidar-radar observations) are feeded into a predefined four-parameter gamma-modified function to calculate ice particle size distributions (PSDs, see Section 2.2). N_{ice} is then calculated by summing up individual ice concentrations over a grid of size bins distributed over the gamma-shaped PSD for the

entire range of observed ice crystal sizes (usually, a continuous integration of the PSD is performed). However, in the ~~in-situ~~ in situ measurements, there are often PSDs that do not contain ice particles < 20 µm, i.e. these size bins are empty. Such PSDs represent aged cirrus after the ice nucleation phase where the smaller ice crystals have grown to larger sizes (see Section 4.3.1). DARDAR-Nice, however, assumes a modified Gamma distribution including all size bins, which partly explains the described positive offset. This behavior was also found by Wolf et al. (2019) who parameterized ~~in-situ and liquid origin~~ in situ-origin and liquid-origin cirrus from balloon-borne measurements by Gamma functions. It is ~~to~~ of note that when subtracting the ice concentrations of the 'empty bins' of ~~in-situ~~ in situ PSDs from the retrieved DARDAR-Nice in a direct intercomparison, the agreement of N_{ice} is improving (not shown here). This is an important finding, as gamma functions are often used to represent cirrus PSDs, both in remote sensing retrieval algorithms and in global models. On the other hand it has to be noted that an offset on the order of a factor of 1.73 is tolerable given the variability of N_{ice} (six orders of magnitude) and other possible error sources in the measurements, both ~~in-situ~~ in situ and remote sensing.

Other assumptions on the PSD shape by the satellite remote sensing method might also contribute to this bias. The PSD shape indeed is provided by 4 parameters, 2 of which are fixed and 2 are retrieved (see Section 2.2). **?** showed that the two fixed PSD parameters defined by Delanoë et al. (2005) and used in DARDAR-Nice might lead to a too steep representation of the small ice mode (i.e. too high N_{ice}) and should be updated in future algorithm versions. Also, the bi-modality of the PSD towards temperature where growth processes become important is not accounted for and usually leads to small positive N_{ice} biases (Sourdeval et al., 2018). The cause of these assumptions are difficult to account for, as they most likely depend on the cloud-type and on the thermodynamical environment, but they should on a first order be reasonably captured by the 1.73 adjustment factor. Higher N_{ice} in DARDAR-Nice towards low temperatures are also not surprising, as Sourdeval et al. (2018) reported that the PSD parametrization used by DARDAR-Nice predicts higher concentrations of small particles ($D_{ice} < 25\,\mu m$) than the ~~in-situ~~ in situ comparative measurements. The overestimation increases with decreasing temperature, as the small ice particles dominate the PSDs more and more. This might be caused by a sharper representation of small ice concentrations in the PSD parametrization in comparison to the ~~in-situ~~ in situ small ice particle measurements below ~210 K.

A further expected difference between the data sets ~~are~~ arises from their detection limits. The lowest N_{ice} that can be detected by the ~~in-situ~~ in situ instruments is $10^{-4}cm^{-3}$, for the highest N_{ice} there is no limitation. Detection limits for DARDAR-Nice depend on lidar-radar sensitivity but are also influenced by the instrumental resolution, which may cause specific features to remain undetected. This effect, however, is represented in Fig. 13 by the 10-s sampling of 1-Hz ~~in-situ~~ in situ PSDs. Indeed, DARDAR-Nice misses the high N_{ice} in the temperature range 210-220 K, but these are young, line shaped contrails which are too small scale to be detected from satellite. Also,

part of the thinnest cirrus are not represented by DARDAR-Nice. This will be further discussed in the next section describing the global N_{ice} distribution from DARDAR-Nice.

Overall, following the above-mentioned arguments, an overestimation within a factor of 2 in DARDAR-Nice by comparison to the ~~in-situ~~ in situ data set is expected, although there is still some uncertainty as to how this overestimation will propagate globally and over various ice cloud regimes. The ratio of 1.73 in N_{ice} between DARDAR-Nice and the ~~in-situ~~ in situ data set, found from Figure 13, should therefore be thought of as a minimum expected bias. Finally, the bias is expected to be stronger at low temperatures than at high temperatures, due to the increased likelihood of missing bins as well as the higher importance of the representation of the small ice particle mode in the PSDs. A correction that depends on temperature, and possibly IWC, might therefore be optimal but a simpler first-order correction of 1.73 for all T and IWC range should here be sufficient for the needs of this study and considering the multitude of processes that can lead to this bias. Future studies will be required to precisely understand such inherent differences between satellite and in situ dataset.

6.2 Global cirrus N_{ice}

The global frequency distribution of N_{ice} from ten years of satellite observations is shown in Figure 14. The data was collected twice a day, approximately at midday and at midnight (satellite equator-crossing time is 1.30 am/pm), from June 2006 to December 2016. Overall, the global satellite data set consists of nearly 2×10^{10} N_{ice} retrievals. The color code represent frequencies of occurrence, the black contours the 25, 50 and 75th percentiles.

From the median (solid black line), a slight increase of N_{ice} with decreasing temperature is visible, which is somewhat different to the ~~in-situ~~ in situ median N_{ice} (solid blue line, from Figure 7, middle left panel), where no temperature dependence is found. The DARDAR-Nice temperature dependence was already noted and discussed by Gryspeerdt et al. (2018). Another difference is that at T $\gtrsim$ 210 K, the maximum N_{ice} of DARDAR-Nice reaches up to 100 cm^{-3}, while the maximum ~~in-situ~~ in situ N_{ice} is only about 10 cm^{-3} (outside of young contrails).

We attribute the slightly increasing median N_{ice} with decreasing temperature to homogeneous ice nucleation events, because homogeneous ice nucleation rates increase with decreasing temperature, but their appearance in space and time is transient, as discussed in Section 4.2.2. Thus, such events are difficult to find by research aircraft. Hence, these events are likely underrepresented in the aircraft observations.

The thinnest cirrus with low N_{ice} are represented by DARDAR-Nice for temperatures $\gtrsim$ 190 K. At $\lesssim$ 190 K, however, a decreasing detectability of thin cirrus becomes ~~visible~~ apparent in the DARDAR-Nice climatology: in contrast to the ~~in-situ~~ in situ climatology, lesser or no thin cirrus are measured with decreasing temperature. The reason is that the colder the cirrus clouds, the smaller are the ice crystals and the lesser their IWC (Figure 10, top and bottom left panel). In the ~~in-situ~~ in situ N_{ice} climatology, in the TTL ($\lesssim$ 205 K), an increased occurrence of very thin cirrus with

N_{ice} around 0.001 cm^{-3} is reported in Section 4.3.1 and explained as aged cirrus consisting of only larger ice crystals. Though this type of clouds is partly missing in the DARDAR-Nice climatology, the median N_{ice} decreases again at these temperatures. This might reflect the frequent presence of aged thin cirrus. Note, however, that the statistics at these temperatures is based on a lower number of observations than at higher temperatures (see Figure 15).

The median N_{ice} across all temperatures of the 10 years DARDAR-Nice climatology is about 0.100 cm^{-3} (Figure 14, plain cyan line). Adjusting this number to the offset factor of 1.73 between DARDAR-Nice and the ~~in-situ~~ in situ observations reported in the previous section yields an ~~in-situ~~ in situ average median of 0.056 cm^{-3} (dashed cyan line, see also Table 3). It is nevertheless important to note that such median is by construction computed assuming that all temperature bins have equal weight. When considering their actual relative occurrence as function of temperature (see Figure 15 and later discussion), the ~~in-situ~~ in situ adjusted global DARDAR-Nice median falls down to 0.046 cm^{-3}. This is still larger than the average median of 0.03 cm^{-3} reported from the N_{ice} ~~in-situ~~ in situ climatology (blue line; from Figure 7). Nevertheless, in the light of the offset between the data sets, the decreasing detectability of thin cirrus by DARDAR-Nice and other sources of error in both methods, the agreement between the DARDAR-Nice and the ~~in-situ~~ in situ N_{ice} climatology is good.

Altogether, both data sets have advantages and disadvantages: DARDAR-Nice has the advantage of the long, global time series where all atmospheric situations above the detection limit showing up at the times of observations are sampled. However, the thinnest cirrus at cold temperatures are not detected. Further, an offset is found between DARDAR-Nice and the ~~in-situ~~ in situ observations. On the other hand, the ~~in-situ~~ in situ N_{ice} climatology is based on a much smaller data set which is randomly distributed between different atmospheric situations. But, nearly the complete range of possible N_{ice} can be detected by the ~~in-situ~~ in situ instruments.

For comparisons with other N_{ice} data sets or results from global models, the percentiles of the adjusted DARDAR-Nice as well as the average ~~in-situ~~ in situ N_{ice} are shown in Figure ~~15~~14 and listed in Table ~~2~~?? ~~(note that an in-situ data set slightly smaller than the data set presented here, but extended with regard to Krämer et al.~~ (note that an in situ data set slightly smaller than the data set presented here, but extended with regard to Krämer et al. (2009) is alre

.

The DARDAR-Nice data set does not only provide the N_{ice} distribution with temperature as shown in Figure 14, but, as it ~~contain~~ contains the entire spatial and temporal N_{ice} information, also the actual appearance of cirrus clouds in the N_{ice}-T parameter space. This is shown in Figure 15, where the occurrences of DARDAR-Nice N_{ice} retrievals are indicated by ~~a~~ the colored background. It can be noticed that, in regions of high frequency of occurrence (for $T \gtrsim 210$ K), the agreement between DARDAR-Nice and the in situ data set is best.

From this portrayal it can be seen that the cirrus clouds do not spread evenly across all temperatures, but that about 50% of the cirrus appear at temperatures above about 225 K (see also Table 3,

temperature range of global 'most frequent' median N_{ice}). This clustering of cirrus at warmer temperatures is likely because ~~in-situ and liquid origin~~ in situ-origin and liquid-origin cirrus clouds are both found in this warmest and lowest cirrus layer, while at colder temperatures and higher altitudes only ~~in-situ~~ in situ-origin cirrus are present (see also Section 3.1 and Figure 3). This vertical structure of the cloud types is also reported from observations by Krämer et al. (2016); Luebke et al. (2016); Wolf et al. (2018), from global modeling by Gasparini and Lohmann (2016)~~(they name liquid origin cirrus 'detrained ice')~~, from satellite and global modeling by Gasparini et al. (2018) and also from 12 years ERA-interim data analysis in the North Atlantic region by Wernli et al. (2016). ~~Wernli et al. (2016) also provides~~

Gasparini et al. (2018) provide global relative frequencies of liquid-origin cirrus with respect to temperature: more than 50% of the cirrus clouds in the range between 235 K and 220 K are of liquid-origin, decreasing rapidly to about 20% between 200 K and 180 K. These findings from satellite observations and global modeling are reasonably consistent with those from trajectory analysis by Wernli et al. (2016), who reported the relative frequencies of ~~liquid origin~~ liquid-origin cirrus with respect to pressure ~~, which decreases~~ to decrease from about 55% of the cirrus at 500 hPa (roughly 240 K), to 50, 30, 5% at 400, 300, 200 hPa (roughly 230, 215, 200 K; see Figure 2).

The analysis presented here provides the information that globally, half of the cirrus are in the lowest, warmest cirrus layer ~~that contains a significant part of liquid origin cirrus .~~ between about 220 K and 240 K, where, as mentioned above, about half of the cirrus are of liquid-origin. This is of importance because of the differing radiative properties of ~~in-situ and liquid origin~~ in situ-origin and liquid-origin cirrus shown in Section 3.1.1 (see Figure 5): if the thick ~~liquid origin~~ liquid-origin cirrus clouds occur with such a high frequency, their strong cooling effect might exceed the much smaller warming effect of the ~~in-situ origin~~ in situ-origin cirrus which could lead to a general cooling by cirrus.

Note that an analysis of N_{ice} in the IWC-T space, similarly to Figure 6, is shown in Figure 5 of the SM. This figure shows a good climatological agreement between the satellite product and the Cirrus Guide II data set, with very similar distribution of N_{ice} in the IWC-T space. Differences could be attributed to lack of statistics in Figure 6 (noisy patterns). However, one notable difference is the slope of the IWC-T relation, which appears much flatter in the satellite product than in the in situ data, as indicated by the density isolines.

6.3 Regional cirrus N_{ice}

Lastly, we provide an impression of the regional variations of N_{ice} (see Table 3). To this end, subsets of the DARDAR-Nice data for five regional latitude bands between 90°, 67.7°, 23.3°, -23.3°, -67.7°, -90°, corresponding to the Arctic, Mid-lat North, the Tropics, Mid-lat South and Antarctica, are considered, and three different N_{ice} medians are computed for each region and for the global data set. A first median (labeled "all Temp.") corresponds to the median N_{ice} value across all temperatures

and considering all temperature bins to be equiprobable, i.e. the same as used in Figure 14. A second (labeled "T-int weighted") represents the median using the relative occurrence of each temperature interval as a weight. The last ("most frequent") shows the most frequently appearing N_{ice}, considering those temperature intervals that contain 50% of the total N_{ice} occurrence; T-range denotes the respective minimum and maximum temperatures (note that in the ~~in-situ~~ in situ data set all three methods would yield to an identical median due to the flat temperature dependence).

Comparing the three median N_{ice}, it is obvious that in most cases the 'T-int weighted' and 'most frequent' medians are smaller than those for 'all temperatures'. This behavior is found because the cirrus clouds appear often at warmer temperatures (see previous subsection) where N_{ice} is moderate, which can be seen particularly in the 'most frequent' medians, where the temperature range of the cirrus occurrence is given.

The global 'most frequent' median N_{ice} is 0.031 cm^{-3} (in comparison to 0.056 and 0.046 cm^{-3} for 'all temperatures' and 'T-int weighted') in the temperature range between 224-242 K (note that, to avoid representing mixed-phase clouds in the DADAR-Nice analysis, 242 K is chosen as maximum temperature). The lowest N_{ice} are found in the Arctic ('most frequent' median 0.016 cm^{-3} between 230-242 K), which is most probably because the updrafts in the Arctic regions are generally lower than in other regions. In Antarctica, the 'most frequent' median is higher (0.029 cm^{-3} between 224 and 242 K). This could be traced back to stronger orographic uplifts in austral winter. The boreal and austral mid-latitude cirrus clouds are similar to the global, with 'most frequent' medians of 0.030 and 0.031 cm^{-3} in the temperature range of 227-242 K. This points to moderate updrafts on average, though regionally orography and convection can cause higher updrafts and high N_{ice}, which is also shown by Sourdeval et al. (2018).

~~The tropical~~ Tropical cirrus clouds are different from those in the other regions. The 'most frequent' cirrus have the highest median (0.074 cm^{-3}) and appear at much colder temperatures (197-221 K), i.e. higher altitudes. This finding corresponds to the ~~in-situ~~ in situ observations presented in Section 3.1 (see Figure 3) and also the DARDAR-Nice analyses of the vertical distribution of N_{ice} shown by Sourdeval et al. (2018). The reason is the strong convection prevailing in tropical regions, lifting ~~liquid origin~~ liquid-origin clouds up to high altitudes and cold temperatures while homogeneously nucleating a large number of ~~in-situ~~ in situ ice crystals in addition (see also Section 5).

For all regions, except the tropics, more than half of the cirrus clouds are found at temperatures warmer than about 225 K and contain a considerable amount of ~~liquid origin~~ liquid-origin cirrus, as discussed in the previous subsection. The same is true in the tropics, but for colder temperatures.

7 Summary and Conclusions

The Cirrus Guide II aims to represent cirrus clouds and their environment from the perspective of in-situ in situ and satellite remote sensing observations. To this end, an in-situ data base in situ database is created, which is based on measurements with state-of the art instrumentation and extended in comparison to earlier studies (Schiller et al., 2008; Krämer et al., 2009; Luebke et al., 2013; Krämer et al., 2016). The in-situ data base in situ database consists now of about 168 hours of ice water content IWC, 9990/8884 hours of ice crystal number concentration N_{ice} and R_{ice}, 11696/320186 hours of in-cloud and clear sky RH_{ice} and, correspondingly, 320186 hours of clear sky water vapor H_2O. The measurements span the altitude range between 5 and 20 km and cover the latitude band from 75 °North to 20 °South. The remote sensing data base database includes 10 years (2006-2016) of global recording of ice crystal number concentrations N_{ice}. The main results form the evaluation of the two data sets are summarized in the following.

1. 7.1 Characteristics and distribution of in-situ origin in situ-origin and liquid origin liquid-origin cirrus (Section 3)

From the extended Cirrus Guide II in-situ in situ data set, we generally *confirm the typical characteristics of the cirrustypes in situ-origin and liquid-origin cirrus* introduced by Krämer et al. (2016) with some additions (see Table 1):

- In-situ in situ-origin as well as liquid origin liquid-origin cirrus consist of two sub-classes determined by the updraft (1:slow updrafts - few large ice crystals form from heterogeneous freezing; 2:fast updrafts - many small ice crystals nucleate homogeneously).
  New in this concept is that also liquid origin liquid-origin cirrus differ in the two updraft regimes. Often, the two subclasses occur in succession and form a bimodal size distribution.

- Liquid origin liquid-origin cirrus are thicker (higher IWC) than in-situ in situ-origin cirrus and are usually characterized by larger ice crystals.

- The differences between the cirrus types are most pronounced in the formation phase of the clouds and are blurred with increasing lifetime due to ice crystal growth and sedimentation or additional ice formation.

In addition, we present a *picture of the distribution of cirrus with respect to altitude and latitude*, including an impression of the vertical structure of liquid origin and in-situ origin liquid-origin and in situ-origin cirrus (Figure 3):

- Across all latitudes, the thicker liquid origin liquid-origin cirrus predominate at lower altitudes, while at higher altitudes the thinner in-situ in situ-origin cirrus prevail. In between, the two cirrus types overlap. This finding is in agreement with Luebke et al. (2016) and Wernli et al. (2016) for mid-latitude and Wolf et al. (2018) for Arctic cirrus.

Finally, a *first estimate of the radiative characteristics of typical ~~idealized in-situ and liquid origin~~ specific and idealized in situ-origin and liquid-origin cirrus scenarios* is given (Figure 5):

- slow ~~in-situ origin~~ in situ-origin cirrus have a small optical depth (τ: 0.001 - 0.05), resulting in a slight net warming effect of not larger than about 1.5 W/m^2.
- the optical depth of fast ~~in-situ origin~~ in situ-origin cirrus is larger (τ: 0.05 - 1), but most of them are also warming (2-10 W/m^2). The thickest fast ~~in-situ origin~~ in situ-origin cirrus at the lowest altitudes can change the sign of their net forcing, they switch to a slight cooling effect.
- ~~liquid origin~~ liquid-origin cirrus have large optical depths (τ: 1 - 12), and consequently exhibit a quite strong net cooling effect (-15 to -250 W/m^2).

~~2.~~ 7.2 Cirrus and humidity in the tropical tropopause layer (TTL) (Section 5)

The new ~~in-situ~~ in situ data set is extended by observations in the tropical TTL outside, but also, for the first time, inside of the Asian monsoon anticyclone. Therefore, we put special emphasis on the analysis of the TTL environment.

TTL cirrus clouds (Figure 11):

- Two types of most likely ~~in-situ~~ in situ formed cirrus are identified in slow large scale updrafts at low temperatures (T $\lesssim$ 205 K, $\Theta \gtrsim$ 355 K). The first is interpreted as young cirrus (N_{ice} around 0.1-1 cm^{-3} $\gtrsim$ 3 µm diameter), the second as aged cirrus (N_{ice} around 0.001 cm^{-3} $\gtrsim$ 20 µm diameter) where the smaller ice crystals have grown to larger sizes.
- The highest N_{ice} (up to 30 cm^{-3} around the cold point tropopause, CPT) and IWC (up to 1000 ppmv around the CPT) are found in deep convective systems in the Asian monsoon. Such systems represent massive ~~liquid origin~~ liquid-origin cirrus (very high IWC) superimposed by a fresh strong homogeneous ~~in-situ~~ in situ ice nucleation event (many small ice crystals $\lesssim$ 20 µm) in fast updrafts.

TTL humidity (Figure 12):

- In the Asian monsoon, in-cloud and clear sky RH_{ice} is higher (often supersaturated around and above the CPT) than in the surrounding tropics. This is caused by a higher amount of H_2O in the Asian monsoon (most frequently 3 to 5 ppmv) in comparison to the tropics outside (1.5 to 3 ppmv).
- Taking saturation at the stratospheric entry of an air mass as set point for water vapor transport to the stratosphere, the transport is underestimated by $\sim$ 10% in regions of weak convective activity (see also Rollins et al., 2016). In convective regions, the underestimation increased to 20-50% in our observations in the Asian monsoon.

– Convectively injected ice over the Asian monsoon CPT ($\Theta \gtrsim 400$ K, $RH_{ice} \lesssim 100\%$) can locally contribute a significant amount of water (up to an IWC of 8 ppmv, in comparison to only 2 ppmv in the surrounding tropics) that might be evaporated and further transported into the stratosphere.

~~3. In-situ~~ 7.3 in situ and satellite climatologies (Sections 4 and 6)

Cirrus Guide II ~~in-situ~~ in situ cirrus and humidity climatologies:

– Median N_{ice}, R_{ice} and RH_{ice} are presented in the IWC-T parameter space (Figure 6).

Distinct patterns are found: N_{ice} form bands parallel to IWC, while R_{ice} are sorted diagonally in the IWC-T space. At tropical cold temperatures, supersaturations occur in thin as well as in thick cirrus.

– The entire extended data set (Figure 7) is compared to the earlier studies ~~listed above (Figure ??~~(Figure 6, SM).

IWC: the median IWC and the core IWC band is the same in both data sets~~.~~, showing that the ~~in-situ~~ in situ IWC measurement techniques are robust and that the IWC is a stable parameter describing cirrus clouds.

RH_{ice}: the overall picture of the in-cloud and clear sky RH_{ice} distributions has also not changed, demonstrating that high altitude water vapor measurements that were under discussion earlier have improved and stabilized.

N_{ice}: an extended view is presented for N_{ice}, which is due to the better lower N_{ice} detection limit and a better mixture of dynamical situation. The new N_{ice}-T percentiles are lower and show no distinct temperature dependence (average 10%, median and 90% N_{ice} percentiles: 0.002, 0.03 and 0.3 cm^{-3}) in comparison to the earlier observations, that show a slight decrease of N_{ice} with temperature and an average median N_{ice} of about 0.1 cm^{-3}.

– The ~~in-situ~~ in situ data set is subdivided into mid-latitude and tropical climatologies (Figures 8 and 9) and typical cirrus and humidity characteristics of the respective regions are presented.

DARDAR-Nice satellite global cirrus N_{ice} climatology
(Figures 14 and 15):

– A global climatology of N_{ice} from 10 years (2006-2016) of satellite observations is provided that can be used for comparison with global models or other data sets.
The N_{ice} from satellite observations are validated by and adjusted to ~~in-situ~~ in situ measurements from a subset of five campaigns of the Cirrus Guide II.

– The global median N_{ice} from satellite observations is almost 2 times higher than the ~~in-situ~~ in situ median and increases slightly with decreasing temperature.

- N_{ice} medians sorted by geographical regions are highest in the tropics, followed by austral/boreal mid-latitudes, Antarctica and the Arctic.

- In the satellite climatologies of N_{ice}, half of the cirrus are located in the lowest, warmest cirrus layer and contain a significant amount of ~~liquid origin~~ liquid-origin cirrus. Their global median N_{ice} is 0.031 cm^{-3}.

- Regarding the frequent appearance of ~~liquid origin~~ liquid-origin cirrus together with strong cooling effect is a motivation to investigate their influence on the overall cirrus radiative feedback on climate in future studies.

Acknowledgments

This paper is dedicated to ~~my~~ our colleague Cornelius Schiller, who passed away much too early in 2012. He was the initiator of the StratoClim project, including the tropical aircraft campaign. Through this campaign, he intended to complement his work on hydration and dehydration in the tropical tropopause layer, based on observations over Brazil, Australia and Africa (Schiller et al., 2009) with measurements over Asia. The campaign took place successfully out of Kathmandu, Nepal, in Summer 2017, after several years of planning and many hurdles that had to be overcome.

References

Afchine, A., Rolf, C., Costa, A., Spelten, N., Riese, M., Buchholz, B., Ebert, V., Heller, R., Kaufmann, S., Minikin, A., Voigt, C., Zöger, M., Smith, J., Lawson, P., Lykov, A., Khaykin, S., and Krämer, M.: Ice particle sampling from aircraft – influence of the probing position on the ice water content, Atmospheric Measurement Techniques, 11, 4015–4031, doi:10.5194/amt-11-4015-2018, 2018.

Bacer, S., Sullivan, S. C., Karydis, V. A., Barahona, D., Krämer, M., Nenes, A., Tost, H., Tsimpidi, A. P., Lelieveld, J., and Pozzer, A.: Implementation of a comprehensive ice crystal formation parameterization for cirrus and mixed-phase clouds in the EMAC model (based on MESSy 2.53), Geoscientific Model Development, 11, 4021–4041, doi:10.5194/gmd-11-4021-2018, https://www.geosci-model-dev.net/11/4021/2018/, 2018.

Baumgardner, D., Jonsson, H., Dawson, W., O'Connor, D., and Newton, R.: The cloud, aerosol and precipitation spectrometer (CAPS): A new instrument for cloud investigations, Atmos. Res., 59-60, 251–264, 2001.

Baumgardner, D., Abel, S. J., Axisa, D., Cotton, R., Crosier, J., Field, P., Gurganus, C., Heymsfield, A., Korolev, A., Krämer, M., Lawson, P., McFarquhar, G., Ulanowski, Z., and Um, J.: Cloud Ice Properties: In Situ Measurement Challenges; Chapter 9 of 'Ice Formation and Evolution in Clouds and Precipitation: Measurement and Modeling Challenges', Meteorol. Monographs, doi:10.1175/AMSMONOGRAPHS-D-16-0011.1, 2017.

Boucher, O., Randall, D., Artaxo, P., Bretherton, C., Feingold, G., Forster, P., Kerminen, V.-M., Kondo, Y., Liao, H., Lohmann, U., Rasch, P., Satheesh, S., Sherwood, S., B., S., Zhang, X.Y.; Eds. Stocker, T., Qin, D., Plattner, G.-K., Tignor, M., Allen, S., Boschung, J., Nauels, A., Xia, Y., Bex, V., and Midgley, P.: Clouds and aerosols. In: Climate Change 2013: The Physical Science Basis. Contribution of Working Group I to the Fifth Assessment Report of the Intergovernmental Panel on Climate Change, Cambridge University Press, Cambridge, United Kingdom and New York, NY, USA, doi:0.1017/CBO9781107415324.016, 2013.

Brewer, A. W.: Evidence for a world circulation provided by the measurements of helium and water vapour distribution in the stratosphere, Quarterly Journal of the Royal Meteorological Society, 75, 351–363, doi:10.1002/qj.49707532603, https://rmets.onlinelibrary.wiley.com/doi/abs/10.1002/qj.49707532603, 1949.

Buchholz, B., B., K., Smit, H., and Ebert, V.: Validation of an extractive, airborne, compact TDL spectrometer for atmospheric humidity sensing by blind intercomparison., Applied Physics B, 110, 249–262, 2013.

Campbell, J. R., Lolli, S., Lewis, J. R., Gu, Y., and Welton, E. J.: Daytime Cirrus Cloud Top-of-the-Atmosphere Radiative Forcing Properties at a Midlatitude Site and Their Global Consequences, Journal of Applied Meteorology and Climatology, 55, 1667–1679, doi:10.1175/JAMC-D-15-0217.1, 2016.

Costa, A., Meyer, J., Afchine, A., Luebke, A., Günther, G., Dorsey, J. R., Gallagher, M. W., Ehrlich, A., Wendisch, M., Baumgardner, D., Wex, H., and Krämer, M.: Classification of Arctic, midlatitude and tropical clouds in the mixed-phase temperature regime, Atmospheric Chemistry and Physics, 17, 12 219–12 238, doi:10.5194/acp-17-12219-2017, 2017.

Delanoë, J., Protat, A., Testud, J., Bouniol, D., Heymsfield, A. J., Bansemer, A., Brown, P. R. A., and Forbes, R. M.: Statistical properties of the normalized ice particle size distribution, Journal of Geophysical Research: Atmospheres, 110, doi:10.1029/2004JD005405, https://agupubs.onlinelibrary.wiley.com/doi/abs/10.1029/2004JD005405, 2005.

Dinh, T., Podglajen, A., Hertzog, A., Legras, B., and Plougonven, R.: Effect of gravity wave temperature fluctuations on homogeneous ice nucleation in the tropical tropopause layer, Atmos. Chem. Phys. Discuss.,, 15, 8771–8799, doi:0.5194/acpd-15-8771-2015, 2015.

Fahey, D., Gao, R., Möhler, O., Saathoff, H., Schiller, C., Ebert, V., Krämer, M., Peter, T., Amarouche, N., Avallone, L. M., Bauer, R., Bozóki, Z., Christensen, L. E., Davis, S. M., Durry, G., Dyroff, C., Herman, R. L., Hunsmann, S., Khaykin, S. M., Mackrodt, P., Meyer, J., Smith, J. B., Spelten, N., Troy, R. F., Vömel, H., Wagner, S., and Wienhold, F. G.: The AquaVIT-1 intercomparison of atmospheric water vapor measurement techniques, AMT, 7, 3177–3213, doi:10.5194/amtd-7-3177-2014, 2014.

Finger, F., Werner, F., Klingebiel, M., Ehrlich, A., Jäkel, E., Voigt, M., Borrmann, S., Spichtinger, P., and Wendisch, M.: Spectral optical layer properties of cirrus from collocated airborne measurements – a feasibility study, Atmos. Chem. Phys. Discuss., 15, 19 045–19 077, doi:10.5194/acpd-15-19045-2015, 2015.

Fu, Q. and Liou, K.: Parameterization of the Radiative Properties of Cirrus Clouds, J. Atmos. Sci., 50, 2008–2025, doi:10.1175/1520-0469(1993)050<2008:POTRPO>2.0.CO;2, 1993.

Fueglistaler, S., Dessler, A. E., Dunkerton, T. J., Folkins, I., Fu, Q., and Mote, P. W.: Tropical tropopause layer, Rev. Geophys., 47, 1–31, doi:10.1029/2008RG000267, 2009.

Gasparini, B. and Lohmann, U.: Why cirrus cloud seeding cannot substantially cool the planet, Journal of Geophysical Research: Atmospheres, 121, 4877–4893, doi:10.1002/2015JD024666, 2016.

Gasparini, B., Meyer, A., Neubauer, D., Münch, S., and Lohmann, U.: Cirrus Cloud Properties as Seen by the CALIPSO Satellite and ECHAM-HAM Global Climate Model, Journal of Climate, 31, 1983–2003, doi:10.1175/JCLI-D-16-0608.1, 2018.

Gryspeerdt, E., Sourdeval, O., Quaas, J., Delanoë, J., Krämer, M., and Kühne, P.: Ice crystal number concentration estimates from lidar–radar satellite remote sensing – Part 2: Controls on the ice crystal number concentration, Atmospheric Chemistry and Physics, 18, 14 351–14 370, doi:10.5194/acp-18-14351-2018, 2018.

Heymsfield, A., Krämer, M., Luebke, A., Brown, P., Cziczo, D., Franklin, C., Lawson, P., Lohmann, U. McFarquhar, G., Ulanowski, Z., and Van Tricht, K.: Ice Formation and Evolution in Clouds and Precipitation: Measurement and Modeling Challenges, Chapter 2: Cirrus Clouds, Eds. Baumgardner, D., McFarquhar, G. and Heymsfield, A., Meteor. Monogr., 58, doi:10.1175/AMSMONOGRAPHS-D-16-0010.1, 2017a.

Heymsfield, A., Krämer, M., Wood, N. B., Gettelman, A., Field, P. R., and Liu, G.: Dependence of the Ice Water Content and Snowfall Rate on Temperature, Globally: Comparison of in Situ Observations, Satellite Active Remote Sensing Retrievals, and Global Climate Model Simulations, JOURNAL OF APPLIED METEOROLOGY AND CLIMATOLOGY, 56, 189–215, doi:10.1175/JAMC-D-16-0230.1, 2017b.

Jensen, E. and Pfister, L.: Transport and freeze-drying in the tropical tropopause layer, J. Geophys. Res., 109, doi:10.1029/2003JD004022, 2004.

Jensen, E., Lawson, P., Baker, B., Pilson, B., Mo, Q., Heymsfield, A., Bansemer, A., Bui, T., McGill, M., Hlavka, D., Heymsfield, G., Platnick, S., Arnold, G., and Tanelli, S.: On the importance of small ice crystals in tropical anvil cirrus, Atmos. Chem. Phys., 9, 5519–5537, 2009.

Jensen, E., Diskin, G., Lawson, P. Lance, S., Bui, T., Hlavka, D., McGill, M., Pfister, L., Toon, O., and Gao, R.: Ice nucleation and dehydration in the Tropical Tropopause Layer , PNAS, 110, 2041–2046, doi:10.1073/pnas.1217104110, 2013a.

Jensen, E., Lawson, P., Bergman, J. W., Pfister, L., Bui, T. P., and Schmitt, C. G.: Physical processes controlling ice concentrations in synoptically forced, midlatitude cirrus, J. Geophys. Res., 118, 5348–5360, doi:10.1002/jgrd.50421, 2013b.

Jensen, E. J. and Ackerman, A. S.: Homogeneous aerosol freezing in the tops of high-altitude tropical cumulonimbus clouds, Geophysical Research Letters, 33, doi:10.1029/2005GL024928, https://agupubs.onlinelibrary.wiley.com/doi/abs/10.1029/2005GL024928, 2006.

Jensen, E. J., Ackerman, A. S., and Smith, J. A.: Can overshooting convection dehydrate the tropical tropopause layer?, Journal of Geophysical Research: Atmospheres, 112, 1407–1413, doi:10.1029/2006JD007943, 2007.

Jensen, E. J., Pfister, L., and Bui, T. P.: Physical processes controlling ice concentrations in cold cirrus near the tropical tropopause, JOURNAL OF GEOPHYSICAL RESEARCH-ATMOSPHERES, 117, doi:10.1029/2011JD017319, 2012.

Jensen, E. J., Pfister, L., Jordan, D. E., Bui, T. V., Ueyama, R., Singh, H. B., Thornberry, T. D., Rollins, A. W., Gao, R.-S., Fahey, D. W., Rosenlof, K. H., Elkins, J. W., Diskin, G. S., DiGangi, J. P., Lawson, R. P., Woods, S., Atlas, E. L., Rodriguez, M. A. N., Wofsy, S. C., Pittman, J., Bardeen, C. G., Toon, O. B., Kindel, B. C., Newman, P. A., McGill, M. J., Hlavka, D. L., Lait, L. R., Schoeberl, M. R., Bergman, J. W., Selkirk, H. B., Alexander, M. J., Kim, J.-E., Lim, B. H., Stutz, J., and Pfeilsticker, K.: THE NASA AIRBORNE TROPICAL TROPOPAUSE EXPERIMENT High-Altitude Aircraft Measurements in the Tropical Western Pacific, BULLETIN OF THE AMERICAN METEOROLOGICAL SOCIETY, 98, 129+, doi:10.1175/BAMS-D-14-00263.1, 2017.

Jones, H., Haywood, J., Marenco, F., O'Sullivan, D., Meyer, J., Thorpe, R., Gallagher, M., Krämer, M., Bower, K., Rädel, G., Rap, A., Woolley, A., Forster, P., and Coe, H.: A methodology for in-situ and remote sensing of microphysical and radiative properties of contrails as they evolve into cirrus, Atmospheric Chemistry and Physics, 12, 8157–8175, doi:10.5194/acp-12-8157-2012, cited By 1, 2012.

Joos, H.: Warm Conveyor Belts and Their Role for Cloud Radiative Forcing in the Extratropical Storm Tracks, Journal of Climate, 32, 5325–5343, doi:10.1175/JCLI-D-18-0802.1, 2019.

Joos, H., Spichtinger, P., Reutter, P., and Fusina, F.: Influence of heterogeneous freezing on the microphysical and radiative properties of orographic cirrus clouds, Atmospheric Chemistry and Physics, 14, 6835–6852, doi:10.5194/acp-14-6835-2014, https://www.atmos-chem-phys.net/14/6835/2014/, 2014.

Kärcher, B. and Lohmann, U.: A parameterization of cirrus cloud formation: homogeneous freezing of supercooled aerosols, J. Geophys. Res., 107, 7433 – 7462, 2002.

Kaufmann, S., Voigt, C., Heller, R., Jurkat-Witschas, T., Krämer, M., Rolf, C., Zöger, M., Giez, A., Buchholz, B., Ebert, V., Thornberry, T., and Schumann, U.: Intercomparison of midlatitude tropospheric and lower-stratospheric water vapor measurements and comparison to ECMWF humidity data, Atmospheric Chemistry and Physics, 18, 16 729–16 745, doi:10.5194/acp-18-16729-2018, https://www.atmos-chem-phys.net/18/16729/2018/, 2018.

Kienast-Sjögren, E., Rolf, C., Seifert, P., Krieger, U. K., Luo, B. P., Krämer, M., and Peter, T.: Climatological and radiative properties of midlatitude cirrus clouds derived by automatic evaluation of lidar measurements, Atmospheric Chemistry and Physics, 16, 7605–7621, doi:10.5194/acp-16-7605-2016, 2016.

Korolev, A.: Limitations of the Wegener–Bergeron–Findeisen Mechanism in the Evolution of Mixed-Phase Clouds , J. Atmos. Sci., 64, 3372–3375, doi:10.1175/JAS4035.1, 2007.

Korolev, A. and Field, P. R.: Assessment of the performance of the inter-arrival time algorithm to identify ice shattering artifacts in cloud particle probe measurements, Atmospheric Measurement Techniques, 8, 761–777, doi:10.5194/amt-8-761-2015, https://www.atmos-meas-tech.net/8/761/2015/, 2015.

Krämer, M., Schiller, C., Afchine, A., Bauer, R., Gensch, I., Mangold, A., Schlicht, S., Spelten, N., Sitnikov, N., Borrman, S., de Reus, M., and Spichtinger, P.: Ice supersaturations and cirrus cloud crystal numbers, ACP, 9, 3505–3522, 2009.

Krämer, M., Rolf, C., Luebke, A., Afchine, A., Spelten, N., Costa, A., Meyer, J., Zoeger, M., Smith, J., Herman, R. L., Buchholz, B., Ebert, V., Baumgardner, D., Borrmann, S., Klingebiel, M., and Avallone, L.: A microphysics guide to cirrus clouds - Part 1: Cirrus types, Atmospheric Chemistry and Physics, 16, 3463–3483, doi:10.5194/acp-16-3463-2016, 2016.

Kübbeler, M., Hildebrandt1, M., Meyer, J., Schiller, C., Hamburger, T., Jurkat, T., Minikin, A., Petzold, A., Rautenhaus, M., Schlager, H., chumann, U., Voigt, C., Spichtinger, P., Gayet, J.-F., Gourbeyre, C., and Krämer, M.: Thin and subvisible cirrus and contrails in a subsaturated environment, ACP, 11, 5853–5865, doi:10.5194/acp-11-5853-2011, 2011.

Lawson, R., O'Connor, D., Zmarzly, P., Weaver, K., Baker, B., Mo, Q., and Jonsson, H.: The 2D – S (Stereo) probe: Design and preliminary tests of a new airborne, high – speed, high – resolution particle Imaging probe, J. Atmos. Ocean. Technol., 23, 1462 – 1477, 2006.

Lawson, R. P., Woods, S., Jensen, E., Erfani, E., Gurganus, C., Gallagher, M., Connolly, P., Whiteway, J., Baran, A. J., May, P., Heymsfield, A., Schmitt, C. G., McFarquhar, G., Um, J., Protat, A., Bailey, M., Lance, S., Muehlbauer, A., Stith, J., Korolev, A., Toon, O. B., and Krämer, M.: A Review of Ice Particle Shapes in Cirrus formed In Situ and in Anvils, Journal of Geophysical Research: Atmospheres, 124, 10 049–10 090, doi:10.1029/2018JD030122, https://agupubs.onlinelibrary.wiley.com/doi/abs/10.1029/2018JD030122, 2019.

Luebke, A., Avallone, L., Schiller, C., Meyer, J., Rolf, C., and Krämer, M.: Ice water content of Arctic, midlatitude, and tropical cirrus – Part 2: Extension of the database and new statistical analysis, ACP, 13, 6447–6459, 2013.

Luebke, A. E., Afchine, A., Costa, A., Grooss, J.-U., Meyer, J., Rolf, C., Spelten, N., Avallone, L. M., Baumgardner, D., and Krämer, M.: The origin of midlatitude ice clouds and the resulting influence on their microphysical properties, Atmospheric Chemistry and Physics, 16, 5793–5809, doi:10.5194/acp-16-5793-2016, 2016.

May, R.: Open – path, near – infrared tunable diode laser spectrometer for atmospheric measurements of H_2O, J. Geophys. Res., 103, 19 161 – 19 172, doi:10.1029/98jd01678, 1998.

McFarquhar, G., Junshik, U., Freer, M., Baumgardner, D., Kok, G., and Mace, G.: The Importance of Small Ice Crystals to Cirrus Properties: Observations from the Tropical Warm Pool International Cloud Experiment (TWP-ICE), Geophys. Res. Lett., 34, doi:10.1029/2007GL029865, 2007.

Meyer, J.: Ice Crystal Measurements with the New Particle Spectrometer NIXE-CAPS, Schriften des Forschungszentrums Jülich. Reihe Energie und Umwelt / Energy and Environment; 160; ISBN:9783893368402, 2012.

Meyer, J., Rolf, C., Schiller, C., Rohs, S., Spelten, N., Afchine, A., Zöger, M., Sitnikov, N., Thornberry, T., Rollins, A., Gao, R., Bozoki, Z., Tatrai, D., Buchholz, B., Ebert, V., Mackrodt, P., Möhler, O., Saathoff,

H., Rosenlof, K., and Krämer, M.: Two decades of water vapor measurements with the FISH fluorescence hygrometer: A review., ACP, 15, 8521–8538, doi:10.5194/acp-15-8521-2015, 2015, 2015.

Mitchell, D. L., Garnier, A., Pelon, J., and Erfani, E.: CALIPSO (IIR–CALIOP) retrievals of cirrus cloud ice-particle concentrations, Atmospheric Chemistry and Physics, 18, 17 325–17 354, doi:10.5194/acp-18-17325-2018, https://www.atmos-chem-phys.net/18/17325/2018/, 2018.

Muhlbauer, A., Ackerman, T., Comstock, J., Diskin, G., Evans, S., Lawson, R., and Marchand, R.: Impact of large-scale dynamics on the microphysical properties of midlatitude cirrus, Journal of Geophysical Research: Atmospheres, 119, 3976–3996, doi:10.1002/2013JD020035, 2014.

Murphy, D. M.: Rare temperature histories and cirrus ice number density in a parcel and a one-dimensional model, Atmospheric Chemistry and Physics, 14, 13 013–13 022, doi:10.5194/acp-14-13013-2014, https://www.atmos-chem-phys.net/14/13013/2014/, 2014.

Pan, L. L., Bowman, K. P., Atlas, E. L., Wofsy, S. C., Zhang, F., Bresch, J. F., Ridley, B. A., Pittman, J. V., Homeyer, C. R., Romashkin, P., and Cooper, W. A.: The Stratosphere-Troposphere Analyses of Regional Transport 2008 (START08) Experiment, Bulletin of the American Meteorological Society, 91, 327–342, doi:10.1175/2009BAMS2865.1, 2010.

Pan, L. L., Atlas, E. L., Salawitch, R. J., Honomichl, S. B., Bresch, J. F., Randel, W. J., Apel, E. C., Hornbrook, R. S., Weinheimer, A. J., Anderson, D. C., Andrews, S. J., Baidar, S., Beaton, S. P., Campos, T. L., Carpenter, L. J., Chen, D., Dix, B., Donets, V., Hall, S. R., Hanisco, T. F., Homeyer, C. R., Huey, L. G., Jensen, J. B., Kaser, L., Kinnison, D. E., Koenig, T. K., Lamarque, J.-F., Liu, C., Luo, J., Luo, Z. J., Montzka, D. D., Nicely, J. M., Pierce, R. B., Riemer, D. D., Robinson, T., Romashkin, P., Saiz-Lopez, A., Schauffler, S., Shieh, O., Stell, M. H., Ullmann, K., Vaughan, G., Volkamer, R., and Wolfe, G.: Convective Transport of Active Species in the Tropics (CONTRAST) experiment, Bull. Amer. Meteor. Soc., 98, 106–128, doi:10.1175/BAMS-D-14-00272.1, 2017.

Penner, J. E., Zhou, C., Garnier, A., and Mitchell, D. L.: Anthropogenic Aerosol Indirect Effects in Cirrus Clouds, Journal of Geophysical Research: Atmospheres, 123, 11,652–11,677, doi:10.1029/2018JD029204, https://agupubs.onlinelibrary.wiley.com/doi/abs/10.1029/2018JD029204, 2018.

Peter, T., Marcolli, C., Spichtinger, P., Corti, T., Baker, M., and Koop, T.: When dry air is too humid, Science, 314, 1399 – 1401, 2006.

Petzold, A., Krämer, M., Neis, P., Rolf, C., Rohs, S., Berkes, F., Smit, H. H., Gallagher, M., Beswick, K., Lloyd, G., Baumgardner, D., Spichtinger, P., Nédélec, P., Ebert, V., Buchholz, B., Riese, M., and Andreas, W.: Upper tropospheric water vapour and its interaction with cirrus clouds as seen from IAGOS longterm routine in-situ observations, Faraday Discussions, 200, 229–249, doi:10.1039/C7FD00006E, http://dx.doi.org/10.1039/C7FD00006E, 2017.

Ploeger, F., Günther, G., Konopka, P., Fueglistaler, S., Müller, R., Hoppe, C., Kunz, A., Spang, R., Grooß, J.-U., and Riese, M.: Horizontal water vapor transport in the lower stratosphere from subtropics to high latitudes during boreal summer, Journal of Geophysical Research: Atmospheres, 118, 8111–8127, doi:10.1002/jgrd.50636, https://agupubs.onlinelibrary.wiley.com/doi/abs/10.1002/jgrd.50636, 2013.

Podglajen, A., Bui, T. P., Dean-Day, J. M., Pfister, L., Jensen, E. J., Alexander, M. J., Hertzog, A., Kärcher, B., Plougonven, R., and Randel, W. J.: Small-Scale Wind Fluctuations in the Tropical Tropopause Layer from

Aircraft Measurements: Occurrence, Nature, and Impact on Vertical Mixing, Journal of the Atmospheric Sciences, 74, 3847–3869, doi:10.1175/JAS-D-17-0010.1, 2017.

Riese, M., Ploeger, F., Rap, A., Vogel, B., Konopka, P., Dameris, M., and Forster, P.: Impact of uncertainties in atmospheric mixing on simulated UTLS composition and related radiative effects, JOURNAL OF GEOPHYSICAL RESEARCH-ATMOSPHERES, 117, doi:10.1029/2012JD017751, 2012.

Righi, M., Hendricks, J., Lohmann, U., Gerhard Beer, C., Hahn, V., Heinold, B., Heller, R., Krämer, M., Rolf, C., Tegen, I., and Voigt, C.: A new approach to simulate aerosol effects on cirrus clouds in EMAC v2.54, GMD Discussion, xx, xxx, doi:xxx, 2019.

Rolf, C., Vogel, B., Hoor, P., Afchine, A., Günther, G., Krämer, M., Müller, R., Müller, S., Spelten, N., and Riese, M.: Water vapor increase in the lower stratosphere of the Northern Hemisphere due to the Asian monsoon anticyclone observed during the TACTS/ESMVal campaigns, Atmospheric Chemistry and Physics, 18, 2973–2983, doi:10.5194/acp-18-2973-2018, https://www.atmos-chem-phys.net/18/2973/2018/, 2018.

Rollins, A. W., Thornberry, T. D., Gao, R. S., Smith, J. B., Sayres, D. S., Sargent, M. R., Schiller, C., Krämer, M., Spelten, N., Hurst, D. F., Jordan, A. F., Hall, E. G., Vömel, H., Diskin, G. S., Podolske, J. R., Christensen, L. E., Rosenlof, K. H., Jensen, E. J., and Fahey, D. W.: Evaluation of UT/LS hygrometer accuracy by intercomparison during the NASA MACPEX mission, JGR, 119, 1915–1935, doi:10.1002/2013JD020817, 2014.

Rollins, A. W., Thornberry, T. D., Gao, R. S., Woods, S., Lawson, R. P., Bui, T. P., Jensen, E. J., and Fahey, D. W.: Observational constraints on the efficiency of dehydration mechanisms in the tropical tropopause layer, Geophysical Research Letters, 43, 2912–2918, doi:10.1002/2016GL067972, 2016.

Sassen, K., Wang, Z., and Liu, D.: Global distribution of cirrus clouds from CloudSat/Cloud-Aerosol Lidar and Infrared Pathfinder Satellite Observations (CALIPSO) measurements, JOURNAL OF GEOPHYSICAL RESEARCH-ATMOSPHERES, 113, doi:10.1029/2008JD009972, 2008.

Schiller, C., Krämer, M., Afchine, A., Spelten, N., and Sitnikov, N.: Ice water content in Arctic, midlatitude and tropical cirrus, J. Geophys. Res., 113, D24208, doi:10.1029/2008JD010342., 2008.

Schiller, C., Grooß, J.-U., Konopka, P., Plöger, F., Silva dos Santos, F. H., and Spelten, N.: Hydration and dehydration at the tropical tropopause, Atmospheric Chemistry and Physics, 9, 9647–9660, doi:10.5194/acp-9-9647-2009, 2009.

Schoeberl, M., Jensen, E., Pfister, L., Ueyama, R., Wang, T., Selkirk, H., Thornberry, T., Dessler, A., and Avery, M.: Water Vapor, Clouds, and Saturation in the Tropical Tropopause Layer, Journal of Geophysical Research: Atmospheres, accepted article, 1–30, doi:10.1029/2018JD029849, 2019.

Schoeberl, M. R., Jensen, E. J., Pfister, L., Ueyama, R., Avery, M., and Dessler, A. E.: Convective Hydration of the Upper Troposphere and Lower Stratosphere, Journal of Geophysical Research: Atmospheres, 123, 4583–4593, doi:10.1029/2018JD028286, 2018.

Sitnikov, N., Yushkov, V., Afchine, A., Korshunov, L., Astakhov, V., Ulanovskii, A., Krämer, M., Mangold, A., Schiller, C., and Ravegnani, F.: The FLASH Instrument for Water Vapor Measurements on Board the High-Altitude Airplane, Instruments and Experimental Techniques, 50, 113121, 2007.

Solomon, S., Rosenlof, K. H., Portmann, R. W., Daniel, J. S., Davis, S. M., Sanford, T. J., and Plattner, G.-K.: Contributions of Stratospheric Water Vapor to Decadal Changes in the Rate of Global Warming, SCIENCE, 327, 1219–1223, doi:10.1126/science.1182488, 2010.

Sourdeval, O., Gryspeerdt, E., Krämer, M., Goren, T., Delanoë, J., Afchine, A., Hemmer, F., and Quaas, J.: Ice crystal number concentration estimates from lidar–radar satellite remote sensing – Part 1: Method and evaluation, Atmospheric Chemistry and Physics, 18, 14 327–14 350, doi:10.5194/acp-18-14327-2018, 2018.

Spichtinger, P. and Cziczo, D. J.: Impact of heterogeneous ice nuclei on homogeneous freezing events, J. Geophys. Res., 115, D14208, doi:10.1029/2009JD012168, 2010.

Spichtinger, P. and Krämer, M.: Tropical tropopause ice clouds: a dynamic approach to the mystery of low crystal numbers, Atmos. Chem. Phys., 13, doi:10.5194/acp-13-9801-2013, 2013.

Spreitzer, E. J., Marschalik, M. P., and Spichtinger, P.: Subvisible cirrus clouds – a dynamical system approach, Nonlinear Processes in Geophysics, 24, 307–328, doi:10.5194/npg-24-307-2017, https://www.nonlin-processes-geophys.net/24/307/2017/, 2017.

Thornberry, T., Rollins, A., Avery, M., Woods, S., Lawson, R., Bui, T., and Gao, R.-S.: Ice water content-extinction relationships and effective diameter for TTL cirrus derived from in situ measurements during ATTREX 2014, J. Geophys. Res., 122, 4494–4507, doi:10.1002/2016JD025948, 2017.

Thornberry, T. D., Rollins, A. W., Gao, R. S., Watts, L. A., Ciciora, S. J., McLaughlin, R. J., and Fahey, D. W.: A two-channel, tunable diode laser-based hygrometer for measurement of water vapor and cirrus cloud ice water content in the upper troposphere and lower stratosphere, Atmospheric Measurement Techniques, 8, 211–224, doi:10.5194/amt-8-211-2015, https://www.atmos-meas-tech.net/8/211/2015/, 2015.

Ueyama, R., Jensen, E. J., and Pfister, L.: Convective Influence on the Humidity and Clouds in the Tropical Tropopause Layer During Boreal Summer, Journal of Geophysical Research: Atmospheres, 123, 7576–7593, doi:10.1029/2018JD028674, 2018.

Urbanek, B., Groß, S., Schäfler, A., and Wirth, M.: Determining stages of cirrus evolution: a cloud classification scheme, Atmospheric Measurement Techniques, 10, 1653–1664, doi:10.5194/amt-10-1653-2017, https://www.atmos-meas-tech.net/10/1653/2017/, 2017.

Urbanek, B., Groß, S., Wirth, M., Rolf, C., Krämer, M., and Voigt, C.: High Depolarization Ratios of Naturally Occurring Cirrus Clouds Near Air Traffic Regions Over Europe, Geophysical Research Letters, 45, 13,166–13,172, doi:10.1029/2018GL079345, 2018.

Vali, G., DeMott, P. J., Möhler, O., and Whale, T. F.: Technical Note: A proposal for ice nucleation terminology, Atmospheric Chemistry and Physics, 15, 10 263–10 270, doi:10.5194/acp-15-10263-2015, https://www.atmos-chem-phys.net/15/10263/2015/, 2015.

Vogel, B., Günther, G., Müller, R., Grooß, J.-U., Afchine, A., Bozem, H., Hoor, P., Krämer, M., Müller, S., Riese, M., Rolf, C., Spelten, N., Stiller, G. P., Ungermann, J., and Zahn, A.: Long-range transport pathways of tropospheric source gases originating in Asia into the northern lower stratosphere during the Asian monsoon season 2012, Atmospheric Chemistry and Physics, 16, 15 301–15 325, doi:10.5194/acp-16-15301-2016, https://www.atmos-chem-phys.net/16/15301/2016/, 2016.

Voigt, C., Schumann, U., Minikin, A., Abdelmonem, A., Afchine, A., Borrmann, S., Boettcher, M., Bucuchholz, B., Bugliaro, L., Costa, A., Curtius, J., Dollner, M., Doernbrack, A., Dreiling, V., Ebert, V., Ehrlich, A., Fix, A., Forster, L., Frank, F., Fuetterer, D., Giez, A., Graf, K., Grooss, J.-U., Gross, S., Heimerl, K., Heinold, B., Hueneke, T., Jaervinen, E., Jurkat, T., Kaufmann, S., Kenntner, M., Klingebiel, M., Klimach, T., Kohl, R., Krämer, M., Krisna, T. C., Luebke, A., Mayer, B., Mertes, S., Molleker, S., Petzold, A., Pfeilsticker, K., Port, M., Rapp, M., Reutter, P., Rolf, C., Rose, D., Sauer, D., Schaefer, A., Schlage, R., Schnaiter, M., Schneider,

J., Spelten, N., Spichtinger, P., Stock, P., Walser, A., Weigel, R., Weinzierl, B., Wendisch, M., Werner, F., Wernli, H., Wirth, M., Zahn, A., Ziereis, H., and Zöger, M.: ML-Cirrus the airborne experiment on natural cirrus and contrail cirrus with the high-altitude long-range research aircraft HALO, Bulletin of the American Meteorological Society, 98, 271–288, doi:10.1175/BAMS-D-15-00213.1, 2017.

Wendisch, M., Yang, P., and Pilewskie, P.: Effects of ice crystal habit on thermal infrared radiative properties and forcing of cirrus, Journal of Geophysical Research, 112, doi:10.1029/2006JD007899, 2007.

Wendisch, M., Poeschl, U., Andreae, M. O., Machado, L. A. T., Albrecht, R., Schlager, H., Rosenfeld, D., Martin, S. T., Abdelmomonem, A., Afchine, A., Araujo, A. C., Artaxo, P., Aufmhoff, H., Barbosa, H. M. J., Borrmann, S., Braga, R., Buchholz, B., Cecchini, M. A., Costa, A., Curtius, J., Dollner, M., Dorf, M., Dreiling, V., Ebert, V., Ehrlich, A., Ewald, F., Fisch, G., Fix, A., Frank, F., Futterer, D., Heckl, C., Heidelberg, F., Hueneke, T., Jakel, E., Jarvinen, E., Jurkat, T., Kanter, S., Kaestner, U., Kenntner, M., Kesselmeier, J., Klimach, T., Knecht, M., Kohl, R., Koelling, T., Krämer, M., Krueger, M., Krisna, T. C., Lavric, J. V., Longo, K., Mahnke, C., Manzi, A. O., Mayer, B., Mertes, S., Minikin, A., Molleker, S., Munch, S., Nillius, B., Pfeilsticker, K., Pohlker, C., Roiger, A., Rose, D., Rosenowow, D., Sauer, D., Schnaiter, M., Schneider, J., Schulz, C., de Souza, R. A. F., Spanu, A., Stock, P., Vila, D., Voigt, C., Walser, A., Walter, D., Weigel, R., Weinzierl, B., Werner, F., Yamasoe, M. A., Ziereis, H., Zinner, T., and Zoeger, M.: ACRIDICON-CHUVA CAMPAIGN Studying Tropical Deep Convective Clouds and Precipitation over Amazonia Using the New German Research Aircraft HALO, BULLETIN OF THE AMERICAN METEOROLOGICAL SOCIETY, 97, 1885–1908, doi:10.1175/BAMS-D-14-00255.1, 2016.

Wernli, H., Boettcher, M., Joos, H., Miltenberger, A. K., and Spichtinger, P.: A trajectory-based classification of ERA-Interim ice clouds in the region of the North Atlantic storm track, Geophysical Research Letters, 43, 6657–6664, doi:10.1002/2016GL068922, https://agupubs.onlinelibrary.wiley.com/doi/abs/10.1002/2016GL068922, 2016.

Wolf, V., Kuhn, T., Milz, M., Voelger, P., Krämer, M., and Rolf, C.: Arctic ice clouds over northern Sweden: microphysical properties studied with the Balloon-borne Ice Cloud particle Imager B-ICI, Atmospheric Chemistry and Physics, 18, 17 371–17 386, doi:10.5194/acp-18-17371-2018, 2018.

Wolf, V., Kuhn, T., and Krämer, M.: On the dependence of cirrus parametrizations on the cloud origin, Geophysical Research Letters, 46, 12 565–12 571, doi:10.1029/2019GL083841, 2019.

Woods, S., Lawson, R. P., Jensen, E., Bui, T. P., Thornberry, T., Rollins, A., Pfister, L., and Avery, M.: Microphysical Properties of Tropical Tropopause Layer Cirrus, Journal of Geophysical Research: Atmospheres, 123, 6053–6069, doi:10.1029/2017JD028068, 2018.

Zondlo, M. A., Paige, M. E., Massick, S. M., and Silver, J. A.: Vertical cavity laser hygrometer for the National Science Foundation Gulfstream-V aircraft, J. Geophys. Res., 115, D02309, doi:10.1029/2010JD014445, 2010.